A study of synchronisation in the classical phase-oscillator model of an electrical power grid

by

CHRISTIAAN OLIVIER

submitted in accordance with the requirements
for the degree of

MASTER OF SCIENCE

in the subject

PHYSICS

at the

UNIVERSITY OF SOUTH AFRICA

SUPERVISOR: Professor A. E. Botha

February 2026

Declaration

Name: Christiaan Olivier

Student Number: 59417471

Degree: Master of Science (Physics)

I declare that the dissertation "The use of classical phase-oscillator models in electrical power systems" is my own work and that all the sources that I have used or quoted have been indicated and acknowledged by means of complete references, and that any use of Artificial Intelligence (AI) has been fully disclosed.

I further declare that I submitted the dissertation to the appropriate originality detection system which is endorsed by Unisa and that it falls within the accepted requirements for originality.

I further declare that I have not previously submitted this work, or part of it, for examination at Unisa for another qualification or at any other higher education institution.

I further declare that where Artificial Intelligence (AI) tools have been used in the preparation of this thesis/dissertation, their use has been limited to ethical permissible support, has been fully disclosed, and does not replace my own original research, my independent critical thinking and analysis, or authorship responsibilities.

I understand that failure to disclose AI use, plagiarism and/or lack of academic integrity may constitute academic misconduct under Unisa's policies.

SIGNATURE

8th of June 2026

DATE

Dedication

To my mother.

Acknowledgments

I wish to express my deepest gratitude to Prof. A. E. Botha for his guidance along this journey. Were it not for his patience and invaluable feedback, I would still have known very little about academic writing. I would also like to extend my sincere thanks to the Department of Physics for paying my M.Sc. registration fees, as well as the various administrators at Unisa, particularly those of the HPC facility, who ably assisted me whenever I had queries.

Finally, I am grateful to my friends and family for their moral support in this time, especially my mother, who passed away during the writing of this dissertation.

Abstract

In this work, we study synchronisation in power grids using a classical phase oscillator model that can be thought of as a variant of the famous Kuramoto model for coupled phase oscillators. In the recent literature, the connection between a Kuramoto-like model and power grids has been made by Filatrella, Nielsen and Pedersen. Here, we will show that this connection goes much further back, to the so-called Classical Model of power grids that was introduced in 1951 by the work of Boast and Rector. We also observe that in 2018, Arinushkin and Anishchenko developed a Kuramoto-like model for power grids in which, for the first time, there appear non-negligible phase-lag parameters as a result of the Kron reduced approximation. Although a single phase-lag (or frustration) parameter had been introduced much earlier in the so-called Kuramoto-Sakaguchi model (from 1986), Arinushkin and Anishchenko were the first to introduce multiple phase-lag parameters into a Kuromoto-like model for power grids. Unfortunately, our attempts to replicate their results soon revealed that they used a too-large, fixed time step for the numerical time integration of their equations, and that this led them to make several erroneous conclusions about the grid which they modelled. Therefore, in Chapter 3, we give a detailed critique of the 2018 paper by Arinushkin and Anishchenko. Then, in a follow-up work by Arinushkin and Vadivasova, from 2021, we observe that use was made of nonlinear damping to control the synchronicity of the Kron reduced grid. In this case, we were able to reproduce all the results of Arinushkin and Vadivasova. We were able to develop a more efficient proportional control scheme, based on the global order parameter. Our proposed control scheme and its results were presented at the 2023 International Conference on Electrical, Computer, and Energy Technologies (ICECET). The resulting conference proceeding is included here, in slightly revised form, as Chapter 4. Finally, in Chapter 5, we provide a brief summary of our main findings and some suggestions for future work.

Key terms: Electrical power grids, Kuramoto model, Frustration, Control methods, Damping, Classical Model, Kron reduction

Contents

Chapter 1

Introduction

In recent decades, there has been a shift towards incorporating alternative power sources into existing power grids. Such sources include those derived from photovoltaic cells and wind, as opposed to those based on traditional fossil fuel and nuclear fission reactions. This shift has resulted in an increased reliance on a large number of small power stations, rather than on a small number of large power stations. The problem of achieving synchronicity in grids composed of a larger number of heterogeneous sources is obviously more challenging than it was in traditional grids. Another problem created by the incorporation of renewable energy sources is the inherent intermittent nature of some of the power sources, like wind turbines. Intermittent renewable energies cannot be inserted easily into full scale engineers' models. Since it is infeasible to test the effects of adding different power sources directly to real power grids, one is forced to rely on specialised mathematical models, like those based on the Kuramoto model, to investigate the viability of such extended networks.

Due to its current technological relevance, power grid modelling has now become a highly competitive field with a vast surrounding literature. To provide a clearer overview of all the various aspects involved, the following literature review has been grouped into the relevant section headings of this chapter.

One of the key requirements to avoid the collapse of power grids, is their ability to operate stably in a synchronous mode. Specifically, the generators in a power network need to be phase-synchronised. This refers to the case where the rotational phase velocities of the generators in the network are all the generators in the network are equal. [1]

In this work, we study the synchronisation of power grids as networks of phase oscillators. In particular, we will consider variants of the Kuramoto model [2]. Since 1975, when Kuramoto developed his now-famous model, the model itself, and numerous variants of it, have been used in a wide variety of fields. Thus, we begin our literature review by discussing some basics about network theory (Sec. 1.1.1), and the Kuramoto model and some of its variants (Sec. 1.1.2). In Sec. 1.1.3, we explain what it means for a power grid to be synchronised, and the different types of synchronisation that can exist. In Sec. 1.1.4, we discuss the effect of frustration on synchronicity within a power grid. Then, in Sec. 1.1.5, we establish an important link between the so-called Classical Model for power grids and the more recent Kuramoto model with inertia and added frustration elements. In Sec. 1.1.6, we discuss some control methods that have been used to establish synchronicity in power grids, including the intelligent (smart) grids that are discussed in Sec. 1.1.7. Next, in Sec. 1.1.8, we consider some of the literature surrounding cascading failures that can occur in certain situations. As an interesting example of non-intuitive network behaviour, in Sec. 1.1.9, we give a brief account of Braess' paradox, before discussing the important question of multistability, in Sec. 1.1.10. Since certain variants of the Kuramoto model have become paradigms for studying the unusual synchronous behaviour, called a Chimera state, Sec 1.1.11 gives a necessary, yet brief, overview of how these states may be related to power grids. For completeness, in Sec. 1.1.12 we discuss briefly the role of stochastic modelling, which goes beyond the scope of the present work. Finally, Section 1.1 ends with a discussion about the availability of real-world data on power networks, as well as examples of software packages that are useful for generating synthetic data.

The main problem statement of this exploratory thesis is provided in Section 1.2.

1.1 Literature Review

1.1.1 Complex Network Theory

Complex networks are ubiquitous in nature and appear in a wide variety of contexts; such as, neural networks [3], food webs [4], metabolic networks [5], networks of movie actors linked by mutual appearances [6], and of course, power grids.

In network theory, a network is simply a collection of nodes and connections. Every connection connects a pair of nodes. Within the context of electrical power grids, the

nodes and connections that make up the network can be characterised as follows.

- Node diversity: Power grids consist of consumer nodes and generator nodes. The amount of power that a node produces or consumes corresponds to its detuning from the reference axis, which typically has a frequency of 50 Hz or 60 Hz, depending on the geographic region.
- Topology: This refers to how the nodes in a network are connected to each other. Sometimes, a network is centralised, as in the case where more traditional power sources such as coal and nuclear are used. In other cases, such as when renewable power sources are integrated into existing networks, the topology becomes more decentralised.
- Connection diversity: Refers to the strength of the coupling between consumer and generator nodes. Power grids generally have a high connection diversity, since the transmission lines connecting generators to consumers can typically range from 400 kV to 220 V.

1.1.2 Kuramoto Model

In 1975, Kuramoto [2] developed a mathematical model for describing the synchronisation of a population of coupled non-linear oscillators. This model has since been applied to numerous fields [7, 8], including:

- Josephson junctions: In 1996, Wiesenfeld et al. [9] discussed how one can apply the Kuramoto model to an array of Josephson junctions. They described two transitions, one to partial synchronisation, and the other to complete phase locking of the array.
- Rhythmic applause: In 2000, Néda et al. [10] wrote a paper on the synchronisation of applause. They studied the phenomenon of an audience transitioning from incoherent, asynchronous clapping to clapping in sync. It was found that this phenomenon could be modeled using the Kuramoto model.
- Laser arrays: In 2003, Vladimirov et al. [11] studied the behaviour of an array of oscillators at some critical coupling strength, above which the system becomes unstable. They discussed how the system could be simplified by reducing it to a phase model, which yields the Kuramoto model.

- Neural networks: In 2007, Cumin and Unsworth [12] described how the Kuramoto model can be adapted to model neural networks. They suggested incorporating time-varying natural frequencies and time-varying coupling strengths in the model to accommodate the adaptive nature of neurons in the brain. Later that year, Maistrenko et al. [13] published a similar discovery regarding the application of the Kuramoto-model to neural networks. In 2021, Berner et al. [14] identified a link between the Kuramoto model as it is applied to neural networks and power grids. Specifically, they proved that phase oscillilator models with inertia are a class of adaptive networks.

The Kuramoto model reads as follows:

$$\dot{\theta}_i = \omega_i + \frac{K}{N} \sum_{j=1}^{N} \sin(\theta_j - \theta_i)$$

There are N oscillators, each categorised by its phase, θ_i, and its natural frequency, ω_i. The coupling strength between oscillators is denoted by K. We consider a network to be synchronised if, for every pair of oscillators i and j in the network, $\theta_i - \theta_j$ is constant. The oscillators are coupled in such a way that they synchronise if their natural frequencies are close to each other and/or the coupling strength is large enough.

Higher order interactions

There have been cases where the effects of higher order interactions were investigated. These include the effects of second- [15, 16] and even third-order [17] interactions. For example, in 2016, Grzybowski et al. [15] studied the effects of second order interactions in the Kuramoto model with inertia, specifically as it pertains to power grids. Additionally, in a 2022 study by Bick et al. [17], they investigated the Kuramoto model in the case of third order interactions.

These typically involve something like the following equation [17]:

$$\begin{aligned}\dot{\theta}_i = \omega_i &+ \frac{K_1}{N}\sum_{j=1}^{N}\sin(\theta_j - \theta_i) \\ &+ \frac{K_2}{N^2}\sum_{j=1}^{N}\sum_{l=1}^{N}\sin(2\theta_j - \theta_l - \theta_i) \\ &+ \frac{K_3}{N^3}\sum_{j=1}^{N}\sum_{l=1}^{N}\sum_{m=1}^{N}\sin(\theta_j - \theta_l + \theta_m - \theta_i)\end{aligned}$$

Kuramoto model with inertia and its application to power grids

In 1997, Tanaka et al. [18, 19] proposed a modified version of the Kuramoto model which accounts for inertia. The papers do not explicitly mention power grids. Rather, they mention the Kuramoto model being applied to Josephson Junctions and biological systems, such as the synchronous firing of Asian fireflies, circadian rhythms, and heart beat generation. In 2008, Filatrella et al. [20] applied a similar model to power grids. They modelled the individual power generators and consumers as oscillators. The model introduced by Filatrella in Eq. (16) in his paper reads as follows:

$$m\ddot{\theta}_i + \beta_i\dot{\theta} = \omega_i + K\sum_{j=1}^{N} a_{ij}\sin(\theta_j - \theta_i) \tag{1.1}$$

The phase θ_i and the natural frequency ω_i are relative to a reference frame rotating at 50Hz or 60Hz, depending on the utility frequency of the power grid. m is the coefficient for the inertial term and β_i is the damping coefficient for the ith oscillator. In the context of power grids, m is related to the mass of the rotors in the generators. The adjacency matrix a_{ij} determines whether two nodes are connected. If the nodes i and j are connected, then $a_{ij} = 1$, if not connected, $a_{ij} = 0$.

1.1.3 Synchronisation

In this work, we use the term "synchronisation" to refer to what is typically called "phase synchronisation". There are however various types of synchronisation. [21] These include frequency synchronisation, phase synchronisation, and full synchronisation.

A network of oscillators is said to be frequency synchronised if the time-averaged frequencies of the oscillators in the network are related by some multiple. Phase synchronisation is a special case of frequency synchronisation where, as mentioned before, the phase differences between the oscillators in the network are constant. Full synchronisation is a special case of phase synchronisation where the phases of all the oscillators in a network coincide. When applied to power networks, the synchronisation of the voltage phases and frequencies of every generator in a grid ensures that the AC signals do not exhibit destructive interference instead of constructive interference. From the perspective of the consumer, this would manifest itself as fluctuations in the amount of power supplied by the grid.

In the context of the Kuramoto model, the term "synchronisation" typically refers to phase synchronisation. We thus use the term in this sense for the remainder of this work. There are many factors that can influence the propensity of a power grid to synchronise, including:

- Intermittency of power sources: Renewable power sources such as wind and photovoltaic cells exhibit fluctuations in their power production due to changing weather conditions. [22] This can impede synchronisation in a power network. The effects of these fluctuations were investigated in a 2016 study by Anvari et al. [22] They proposed using time-delay feedback control as a solution.

- Network topology: This includes decentralised topologies, which are typical when renewable sources are integrated into a power grid. In a 2012 paper by Rohden et al. [23], they discussed the advantages and disadvantages of a decentralised grid. It was found that, although decentralised grids are more vulnerable to dynamical perturbations, they are more resistant to topological failures. In 2014, the same authors [24] discussed the benefits of decentralising a power grid with lower transmission line capacities. They found that centralised networks require higher coupling strengths to achieve spontaneous synchronisation than decentralised networks.

- Frustration: In the context of Kuramoto-like models, frustration refers to a phase-lag added to the sinusoidal coupling term. Frustration tends to prevent a network from synchronising. [25] In 2023, Botha et al. [25] investigated the effects of frustration on a network of 500 oscillators by adding frustration to the coupling term through a single parameter. They found that adding frustration brought about strong hysteresis and multistability in a power grid. That being said, under certain circumstances, frustration may actually help induce synchronisation [26].

A common measure of the degree to which a network is synchronised is the order parameter [27]. It is typically defined by the following equation:

$$r = \frac{1}{N}\Big|\sum_{k=1}^{N} e^{i\theta_k}\Big| \tag{1.2}$$

The order parameter, r, is equal to 0 when the network is completely desynchronised, and $r = 1$ when the network is fully synchronised.

1.1.4 Frustration

In 1986, Sakaguchi et al. [28] developed what would later be known as the Kuramoto-Sakaguchi model. They added a phase shift, δ, in the sinusoidal coupling term of the original Kuramoto model, leading to the equation

$$\dot{\theta}_i = \omega_i + \frac{K}{N}\sum_{j=1}^{N}\sin(\theta_j - \theta_i + \delta), \text{ where } |\delta| \leq \frac{\pi}{2}. \tag{1.3}$$

The added parameter, δ, is called the phase-lag or frustration. The term frustration dates back to a 1983 study by Teitel and Jayaprakash [29] on phase transitions in frustrated two-dimensional XY models. In the context of the Kuramoto model, it can be thought of as a phase-lag in the coupling between oscillators. In 2015, Nishikawa and Motter [30] discussed the effects of frustration on power grids. They noted that it is related to the admittance of the transmission lines. However, they described these effects as negligible since the impedances of the transmission lines in a real power grid would be almost purely inductive. In 2023, Botha et al. [25] investigated the propensity of a power grid to synchronise at different levels of frustration and coupling strength. They argued that, despite being typically small in power grids, frustration should not be neglected, since even very small levels of frustration have been shown to affect the behaviour of a neuronal network [3, 31]. It was found that adding frustration to a dilute power grid generally impedes its synchronisation, as one might expect.

Some of the few publications that have addressed the effects of frustration on power networks were written by Arinushkin et al. [32–34] In 2018, Arinushkin and Anishchenko [32] incorporated frustration in their analysis of a power grid by introducing an admittance matrix. This allows one to specify the admittance for each transmis-

sion line in a grid and, consequently, the frustration in the coupling term for each link in the network. They obtained their data from the MATPOWER software package (https://github.com/MATPOWER/matpower). They then applied what is known as Kron reduction, which yielded a smaller matrix describing a simplified system. See Chapter 3 for a critique of this paper.

Although the presence of frustration typically makes a network less likely to synchronise, strategically adding frustration as a form of feedback control can aid in the synchronisation of a network. For example, in a proceeding we wrote in 2023, [26] we investigated the effects of adding frustration to networks of oscillators. The proceeding was based on an article by Arinushkin and Vadivasova [33] where they applied damping as a control method to induce synchronisation in a network. In our case, we applied proportional control such that the frustration was varied according to the order parameter of the network. The more asynchronous the network was, the more frustration was added. We found that in certain cases frustration can make an otherwise bi-stable network synchronous or asynchronous. Bi-stability refers to the case where a network may or may not synchronise, depending on the initial conditions. In other words, frustration can make a network less sensitive to initial conditions.

1.1.5 Classical Model

The basic generator–load model underlying the Kuramoto approach was already studied in detail by Francesco Tricomi [35] in 1933. The model is equivalent to a Josephson junction and to a pendulum. Although the original paper was written in Italian, it can be appreciated that the fundamental results of the running phase that amounts to a linear term plus some periodic function, with a period uniquely determined by the speed of the linear term, is rigorously derived in Eq. (31) through time normalization (29).

Although Filatrella et al. [20] were the first to make an explicit link between the Kuramoto model with inertia [18, 19] and power grids, this connection, in fact, goes much further back. In 1951, Boast and Rector [36] applied the system of swing equations,

$$
\begin{aligned}
M_1\frac{d^2\delta_1}{dt^2} &= P_{i1} - E_1^2 Y_{11}\cos\theta_{11} - E_1E_2Y_{12}\cos(\theta_{12}-\delta_1+\delta_2) - \ldots \\
&\qquad - E_1E_nY_{1n}\cos(\theta_{1n}-\delta_1+\delta_n) \\
M_2\frac{d^2\delta_2}{dt^2} &= P_{i2} - E_2^2 Y_{22}\cos\theta_{22} - E_2E_1Y_{21}\cos(\theta_{21}-\delta_2+\delta_1) - \ldots \\
&\qquad - E_2E_nY_{2n}\cos(\theta_{2n}-\delta_2+\delta_n) \\
M_n\frac{d^2\delta_n}{dt^2} &= P_{in} - E_n^2 Y_{nn}\cos\theta_{nn} - E_nE_1Y_{12}\cos(\theta_{n1}-\delta_n+\delta_1) - \ldots \\
&\qquad - E_nE_{n-1}Y_{n(n-1)}\cos(\theta_{n(n-1)}-\delta_n+\delta_{n+1})
\end{aligned}
\tag{1.4}
$$

to a "multimachine system".

They derived this system of equations from a system proposed by Kimbark [37] in 1948. The system of equations (1.4) is a generalisation of Eq. (1.1) and Eq. (1.3) . Furthermore, it is more general, since it includes non-uniform inertial terms, coupling strengths, and phase-lags (frustration). In the literature on power grids, the model developed by Boast and Rector has become known as the Classical Model. Thus, in a mathematical sense, the Kuramoto model can be viewed as a special case of this Classical Model model.

1.1.6 Control schemes

Power grids, in general, routinely rely on different forms of external control to prevent instabilities from developing into catastrophic failures. The forms of external intervention can range from manual switching to those based on data gathered by sensors in so-called smart grids. However, one can apply some sort of internal control method to a network to allow it to synchronise. In the case of power networks, one must consider how these control methods may be practically implemented. Various methods have been proposed for facilitating synchronisation in a network of oscillators, such as:

- Proportional control via damping: In 2021, Arinushkin and Vadivasova [33] discussed the application of proportional control via damping to the Kuramoto with inertia. The amount of damping applied was varied depending on the order parameter (r in Eq. (1.2)). Although this can be a very effective means of aiding in synchronisation, it does have the drawback of introducing dissipation in the network.

- Proportional control via a phase-lag (frustration): In a 2023 proceeding [26], we studied proportional control via phase-lag. We applied this control method the same system that was studied in the paper by Arinushkin and Vadivasova [33]. We also varied the phase-lag depending on the order parameter. This type of control can be practically realised by adding capacitance to a line.
- Time-delayed feedback control: In 2016 Anvari et al. [22] proposed using time-delayed feedback as a method of control for fluctuations due to intermittent power sources in a grid. Practically, this involves adding some sort of energy storage system, like a battery, to the network.

1.1.7 Intelligent (smart) grids

The integration of various technologies into modern power grids has led to the emergence of the smart grid. Many of the defining characteristics of smart grids were discussed in a 2012 survey by Fang et al. [38] They described these new and improved digital grids as using two-way flows of electricity and information to form an adaptive, self-healing, distributed network of generators and consumers. In a 2017 study by Morello et al. [39], they described the use of advanced sensing systems and smart sensors to monitor the state of a power network. Based on this information, one could then apply some type of external control to the network. In other words, smart grids can react in real time to changes in power consumption and generation. In more conventional grids, manual monitoring is generally used.

One of the defining features of smart grids is the integration of renewable power sources. [40], which leads to them having a a decentralised topology. In 2014, Pagani and Aiello [41] studied the evolution of complex network topologies in smart grids. They described how the decentralised nature of smart grids could facilitate a decentralised energy market.

Security and vulnerability to attack

There are also drawbacks associated with smart grids. Due to their digital nature, they are more vulnerable to cyber attacks than conventional power grids. In 2011, Mohsenian-Rad and Leon-Garcia [42] categorised cyber attacks as attacks targeting generators, consumers, and distribution & control. The latter type of attacks disrupt

the systems that monitor and control the power grid. An example can be seen in a 2012 paper by Rahman and Mohsenian-Rad [43], in which they investigated the vulnerability of smart grids to false data injection attacks. In another paper on false data injection attacks by Liu et al. [44], they discuss how these attacks involve the injection of erroneous data into smart grid monitoring systems. They described how attackers can introduce arbitrary errors in the state variables of a power grid, leading to faulty state estimations.

In addition to cyber attacks, there are also other types of attacks to consider, such as, for example, electricity theft [45]. In 2019, Li et al. [46] discussed how one can mitigate the losses caused by electricity theft. They suggested the use of some type of deep learning model with which electricity theft could automatically be detected. This type of theft can take the form of fraud, unpaid bills, billing irregularities, or simply physically stealing the electricity with illegal connections [45].

1.1.8 Network Cascades

A cascading failure (also known as a network cascade) is a phenomenon in which a relatively small event triggers a chain reaction that leads to the failure of a large part of a network [47]. These cascades can have significant consequences in the real world. Therefore, developing models to identify the portions of a network that are vulnerable to these triggers has been an area of interest [48–51].

The vulnerability of some part of a grid is related to its topology. In 2019, Schäfer and Yalcin [52] discussed the topological features that typically lead to network cascades. They found that centralised networks are more likely to trigger these types of failures than decentralised ones. This was also confirmed in a 2017 article by Yang et al. [53], in which they discussed how small but topologically central portions of a network are more vulnerable to large network cascades.

In 2016, Witthaut et al. [54] classified links as critical or stable based on their redundant capacity. This is a measure of how much power the network can reroute through nearby links if a link fails. Links that have a low redundant capacity are referred to as critical. These links make ideal targets for attacks since their failure typically triggers a cascading failure in a network.

1.1.9 Braess' Paradox

The phenomenon now known as Braess' paradox was originally observed by D. Braess in his 1968 paper on traffic planning ([55], originally in German, but translated to English in 2005 [56]). As noted by Witthaut and Timme [57] in a 2012 paper, Braess found that closing a road in a traffic network can alleviate traffic congestion rather than exacerbating it. In their paper, Witthaut and Timme [57] observed that Braess' paradox also applies to power networks. They found that, although adding links to a network *usually* enhances the stability of a network, the addition of a specific link may actually have a destabilising effect.

1.1.10 Multistability

Sometimes, a network can have multiple steady states, in which case there is a risk of a sudden transition between states occurring [58]. In the context of power grids, these transitions can correspond to blackouts. This phenomenon is referred to as multistability. The existence of these states have historically been difficult to determine analytically. Thus, they have generally been identified numerically. In 2017, Manik et al. [59] investigated multistability in networks using the Kuramoto model and swing equation dynamics. They presented an algorithm to compute all the phase-synchronised states of a network, both stable and unstable. In 2019, Balestra et al. [58] presented an analytical method for finding the multistability in lossy power grids and oscillator networks. At the time, analytic results for multistability were limited to idealised networks with negligible Ohmic losses, or networks with radial topologies without loops.

1.1.11 Chimera States

In 2002, Kuramoto and Battogtokh [60] investigated the "coexistence of coherence and incoherence in non-locally coupled phase oscillators". This refers to the phenomenon where some of the oscillators in a homogeneous network are synchronised, whilst the rest of the oscillators behave chaotically. In 2004, Abrams and Strogatz [61] described the same phenomenon and referred to it as a chimera-state. These states occur when the network is neither globally (all-to-all) nor locally coupled. It requires some sort of non-local coupling, i.e. networks where the coupling strength decays with distance between oscillators. [62]. Furthermore, it should be noted that the oscillators need to

be identical and frustration needs to be present for a chimera state to occur.

In 2015, Olmi et al. [63] observed intermittent chimera states in otherwise synchronised networks of oscillators modelled using the Kuramoto model with inertia. Later that year, Olmi [64] studied these networks for different values of inertia. She found that intermittent chimera states occur only at large inertia, whilst small inertia yielded quasi-periodic chimeras. In 2024, Deng and Ódor [65] explained how the European high-voltage power grid network can exhibit behaviour that they refer to as "chimera-like states", and which occur in heterogeneous networks. In these heterogeneous networks, the chimera-like states occur without the usual phase-lag parameters [65].

1.1.12 Stochastic Models

In recent years, renewable power sources have been integrated into power grids. The variability in power output from these sources exacerbates the already stochastic stochastic nature of power grids due to the variability in user demand, disrupting the operation of a grid. In 2018, Tumash et al. [66] discussed the effects of intermittent power sources on a grid. The grid was modelled using a Kuramoto model with inertia. They simulated intermittent power sources by adding Gaussian white noise to the network. Depending on the intensity of the noise added, this induced a frequency-locked state, chimera state, or even aided in the synchronisation of a network. In fact, transient events in the order of seconds can lead to failures in large parts of a grid. [67] The magnitude of these disturbances can depend on response times, repair times, and, in the case of renewable power sources, even weather. For example, in 2018, Haehne et al. [68] showed that even atmospheric turbulence can cause disruptions in a network.

1.1.13 Data Availability

Data related to power grids can be categorised as real-world data or synthetic data.

Real-World Data

Real-world data related to power grids are relatively scarce. Many articles use data that are not publicly available. Examples of open-source datasets on power grids include the following:

- Main continental European transmission network: In 2013, Hutcheon and Janusz [69] presented an updated model for a power flow model of the main continental European transmission network. (http://www.powerworld.com/bialek)
- US power grid: There exists an open source dataset for the US power grid (http://www.konect.cc/networks/opsahl-powergrid/).
- Nordic power grid: In 2021, Kumar et al. [70] presented an open-source model of the Nordic transmission grid.
- European high-voltage power grid: There exists a dataset, known as SciGrid, on the European high-voltage power grid. (https://www.power.scigrid.de/pages/downloads.html)

Synthetic Data

There have been cases where realistic networks were generated based on synthetic data. In 2016, Wang et al. [71] presented an algorithm for generating synthetic power system data with what they call "small-world electric" topologies. In the same year, Elyas and Wang [72] conducted a statistical analysis of transmission line capacities. The synthetic data in these cases were derived from real-world data.

A number of software packages have been written to simulate power networks. These include:

- PowerDynamics.jl: In 2022, Plietzsch et al. [73] presented an experimentally validated free, open-source software package written in Julia for the dynamical analysis of power grids. (https://github.com/JuliaEnergy/PowerDynamics.jl)
- Powerfactory: A program that allows the user to conduct real-time simulations of power systems, including distributed power systems. (https://www.digsilent.de/en/powerfactory.html)
- Powerworld: A wide range of products used by transmission planners, power marketers, system operators. (https://www.powerworld.com)
- Matpower: A software package of free, open-source MATLAB-language functions for simulating and optimising steady-state power system problems. (https://github.com/MATPOWER/matpower)

- Simulink: A program developed by Mathworks to simulate power systems. (https://www.mathworks.com/products/simulink.html)

We also investigated test systems as possible sources of data on power grids, including line impedances and power generated. A test system is a reference system to which other power system benchmarks are compared. Its purpose is to test reliability evaluation techniques. It is not a typical system. Rather, it is a hybrid of the different power systems one may encounter. One of the most commonly used test systems is the IEEE Reliability Test System - 1996, also known as RTS-96 [74]. It is an updated version of an older test system, RTS-79 [75]. RTS-96 includes extensive information such as line lengths, line voltages, weekly peak load, bus types, etc. In a 2019 review article by Peyghami et al. [76], they mention several test systems, each with its own niche applications. Unfortunately, these systems did not provide the data we were looking for.

1.2 Problem Statement

The purpose of this work is to explore how classical phase-oscillator models, including variants of the Kuramoto model, have been used in recent times to study the synchronicity in power grids. In particular, we will make use of the Kuramoto model with inertia and added frustration element to investigate under what circumstances simplified models of power grids may, or may not, synchronise.

During the course of our literature review, we have already identified the similarities between Kuramoto-like models which are currently being used to model power grids, and the system of swing equations (Eq. (1.4)), already proposed by Boast and Rector [36] in 1951. As we have shown, this Classical Model is essentially the same as the Kuramoto model with inertia [18, 19]. Although the latter model dates back to the late 1990's, it was not directly linked to studies of power grids until much later (2008) [20]. Interestingly, when Kuramoto developed his model in the 1970's, he was apparently unaware of the more general Classical Model [36] that already existed for power grids. In retrospect, and perhaps in a mathematical sense only, the Kuramoto model can be viewed as a special case of the Classical model.

In what follows, we show that some of the results given in the 2018 paper by Arinushkin and Anishchenko [32], for a reduced system of three generators, are in fact incorrect. Here, we have chosen to concentrate on this work because it is one of the

few works in which the phase-lag (frustration) parameters are non-negligible due to the reduction scheme that was used to simplify the model. Details about this scheme and other mathematical aspects that are relevant to this dissertation are provided in Chapter 2. In Chapter 3, we specifically show that Arinushkin and Anishchenko [32] made use of a too-large, fixed time-step in their numerical time integration method. This introduced noise in the plots, which led them to make several erroneous conclusions about the simplified grid which they studied. We recreated their simulations using a proper numerical time-integration method. This method ensures proper convergence of the numerical solution and highlights the importance of always cross-checking the accuracy of any obtained numerical solutions.

In Chapter 4, we evaluate various methods of control on a network of ten generators, based on the 2021 paper by Arinushkin and Vadivasova [33]. We test the efficacy of varying damping and varying phase-lag as control methods to establish and maintain synchronisation in a relatively small grid ($N = 10$). Most of the material in Chapter 4 has been published in Ref. [26], i.e., the proceedings of the 2023 International Conference on Electrical, Computer and Energy Technologies (ICECET), at which the work was presented.

Chapter 5 concludes the dissertation by summarising and discussing the main findings, as well as suggesting possible avenues for future research in this highly-competitive field.

Chapter 2

Methods

2.1 Introduction

In this chapter, we provide a more detailed description of the mathematical models and methods that form the basis for the simulations that are performed in the subsequent chapters. We begin with a short overview following the description of phase reduction theory given by Nakao [77]. Phase reduction refers to a scheme used to reduce the description of multi-dimensional limit cycle behaviour down to a single dynamical variable, which we refer to as its phase. One can apply phase reduction to a power generator to reduce it to a phase oscillator where the phase refers to the phase of the AC voltage being output by the generator. It follows that one can reduce a power network to a network of phase oscillators. This allows one to model power grids using variants of the famous Kuramoto model [2]. Next, we introduce the basic terminology from network theory that is required to describe power grids. We then discuss Kron reduction theory. Kron reduction allows us to simplify a complex network by reducing the number of nodes. [78] This leads to the optimised model that was used by Arinushkin et al. [32, 33], which we examine in more detail in Chapter 3. The chapter ends with a discussion on the computational methods one can use to speed up these simulations.

2.2 Phase reduction theory

The state of a system can be represented as an M-dimensional state space

$$\mathbf{X} = (X_1, .., X_M)$$

where $\mathbf{X}$ is a real vector [77]. The dynamics of the system can then be described by

$$\frac{d}{dt}\mathbf{X}(t) = \mathbf{F}(\mathbf{X})$$

where t is the time and

$$\mathbf{F}(\mathbf{X}) = (F_1(\mathbf{X}), ..., F_M(\mathbf{X}))$$

is a vector field that depends on $\mathbf{X}$. Note that, for our purposes, we are only considering autonomous systems. Thus, $\mathbf{F}$ does not explicitly depend on t. We say that $\mathbf{X}_0(t)$ is a point in a periodic orbit if there exists some T, such that $\mathbf{X}_0(t+T) = \mathbf{X}_0(t)$, where T denotes the period of the orbit. The natural frequency of the system would then be defined as $\omega = 2\pi/T$.

If the periodic orbit is in a neighbourhood where there are no other periodic orbits, we refer to it as a limit cycle [79]. It follows that limit cycles must be either attractive or repulsive, but for our purposes we will only consider the case where they are attractive. In Fig. 2.1, we see an example of an attractive limit cycle. The presence of a limit cycle in a state space allows us to define the phase θ of a point $\mathbf{X}$ with the function $\Theta(\mathbf{X})$ where

$$\theta = \Theta(\mathbf{X}) \text{ and } 0 \leq \theta < 2\pi.$$

We can define Θ by firstly defining it on the limit cycle as

$$\Theta(\mathbf{X}_0(t)) = \omega t \pmod{2\pi}.$$

We can extend the domain of Θ to the rest of the basin of attraction by defining $\Theta(\mathbf{X}(t))$ to be equal to $\Theta(\mathbf{X}_0(t))$ whenever $\mathbf{X}(t)$ converges to $\mathbf{X}_0(t)$ as $t \to \infty$.

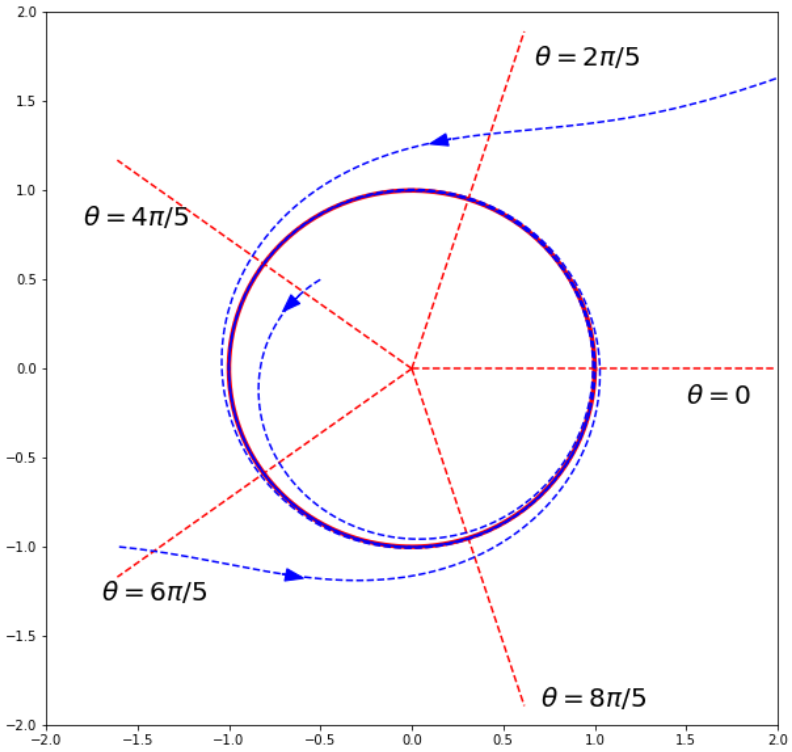

Figure 2.1: An example of a limit cycle. The limit cycle (the red circle) lies in a basin of attraction such that the trajectories (blue) in that basin converge towards it. (Wikipedia contributors, November 27 2025. *Limit cycle*. Wikipedia. https://en.wikipedia.org/wiki/Limit_cycle)

Phase reduction can be used to reduce various complex systems found in nature. For example, in his original work, Kuramoto [2] applied phase reduction to a "temporarily organised" chemical system by modelling it as an ensemble of macroscopic phase oscillators. Phase reduction has also been applied to neuroscience. In 2007, Maistrenko et al. [13] used phase reduction to obtain a simplified model of neuronal dynamics. They then applied the Kuramoto model with synaptic plasticity to investigate the multistability of systems of neurons. In their paper, rather than keeping track of the spike in the voltage of the neuron (as is typical in neuronal models), they reduced the state the neuron to a single phase. Coincidentally, in the same year, Ren and Zhao [80] conducted a similar study on a system of phase oscillators representing a neurological system.

Another example of a system that is amenable to phase reduction is that of a power generator. Like a neuron, a power generator is also a very complicated nonlinear system. [81] One could apply phase reduction to such a system by defining the phase as quite literally being equal to the phase of the output voltage of the AC signal of the generator. In that case, the phase would depend on the power generated by the generator itself, as well as the load (complex impedance) imposed by whatever the generator is connected to.

2.2.1 Link to power grids

Since a power generator can be reduced to a phase oscillator, it follows that a network of power generators (in other words, a power grid) can be reduced to a network of phase oscillators. Such networks can be studied through the lens of network theory.

For those not familiar with the network terminology, we provide some textbook definitions by Harris [82]:

Node: (or in graph theory, a vertex) A connection point in a network.

Edge: (or in graph theory, an edge) A connection between a pair of nodes.

Node degree: The number of edges connected to a node. (See Fig. 2.2)

Average node degree: The sum of the node degrees of all the nodes in the network divided by the number of nodes in the network.

Path: A sequence of edges that connects nodes in a particular order.

Distance: The minimum possible number of edges in a path connecting a pair of nodes.

Global (all-to-all) coupling: A network is globally coupled (all-to-all) if there is an edge connecting every pair of nodes in the network. That is, each node is connected to every other node in the network.

Cluster: A subnetwork of nodes and edges with a higher average node degree than the average node degree of the whole network. Quantitatively, clustering is measured by the clustering coefficient. (See the equation for the clustering coefficient in section 1.2.3 of Harris' book. [82])

Small world network: A network with a high clustering coefficient and low distances.

When applied to power grids, each node corresponds to a power generator, while the edges between nodes correspond to power lines. We model the phase of the rotor in the corresponding power generator. Fig. 2.2 represents a network of 10 oscillators.

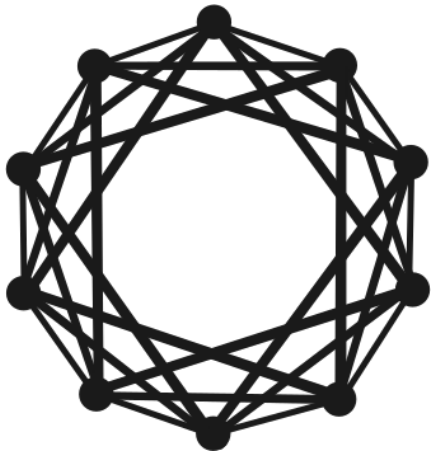

Figure 2.2: A network of 10 nodes for which every node has a degree of 6.

In reality, the topologies of power grids are not quite as regular as portrayed above. Rather, there tend to be some random connections present. Thus, they can be classified as small-world topologies. [83]

2.2.2 Basic definitions

The impedance of an electrical circuit can be defined by the equation $Z = R + jX$, where the complex quantity, Z, is the impedance, R is the resistance, and X is the reactance. X is made up, in general, of the capacitive reactance and the inductive reactance such that $X = X_L - X_C$, where X_L is the inductive reactance and X_C is the capacitive reactance. These quantities are related to the inductance and capacitance by the formulae

$$X_L = 2\pi f L \quad \text{and} \quad X_C = \frac{1}{2\pi f C}.$$

Note that both X_L and X_C depend on the frequency of the applied voltage. The voltage leads the current by the phase of the impedance, ϕ, given by

$$\phi_Z = \arctan\left(\frac{X}{R}\right).$$

The admittance, Y, refers to the reciprocal of the impedance, that is $Y = 1/Z$. Voltage (V), current (I), and admittance (Y) are related by $I = YV$. It follows that the phase of the admittance is given by

$$\phi_Y = -\phi_Z = -\arctan\left(\frac{X}{R}\right)$$

In other words, the phase of the admittance, ϕ_Y, indicates how much the current leads the applied voltage.

2.2.3 Kron Reduction

We can represent the admittance of the connections between nodes in an electrical network with an admittance matrix $\mathbf{Y}$, where the admittance between nodes j and k is denoted by Y_{jk}. Note that this is a symmetrical matrix of dimensions $n \times n$ where n is the number of nodes in the network. The currents, voltages, and admittances between the different nodes are related by the by the matrix equation

$$\mathbf{I} = \mathbf{YV} \tag{2.1}$$

where $\mathbf{I}$ and $\mathbf{V}$ are $n \times 1$ column matrices representing the currents and voltages. [78] Suppose that we have a network where the current in some of the nodes are zero. To perform Kron reduction, we firstly rearrange the nodes such that the lowest entries of $\mathbf{I}$ are zero. Next, we rewrite Eq. (2.1) as

$$\begin{bmatrix} \mathbf{I}_A \\ \mathbf{I}_X \end{bmatrix} = \begin{bmatrix} \mathbf{K} & \mathbf{L} \\ \mathbf{L}^T & \mathbf{M} \end{bmatrix} \begin{bmatrix} \mathbf{V}_A \\ \mathbf{V}_X \end{bmatrix}$$

where every entry of $\mathbf{I}_X$ is zero.

It follows that

$$\mathbf{I}_A = \mathbf{KV}_A + \mathbf{LV}_X \tag{2.2}$$

$$\text{and } \mathbf{I}_X = \mathbf{L}^T\mathbf{V}_A + \mathbf{M}\mathbf{V}_X. \tag{2.3}$$

Subtract $\mathbf{L}^T\mathbf{V}_A$ from both sides of Eq. (2.3) and then multiply both sides by $\mathbf{M}^{-1}$ on the left, taking into account that $\mathbf{I}_X$ is zero. This yields

$$-\mathbf{M}^{-1}\mathbf{L}^T\mathbf{V}_A = \mathbf{V}_X.$$

Substitute the above expression for $\mathbf{V}_X$ into Eq. (2.2).

$$\begin{aligned}\mathbf{I}_A &= \mathbf{K}\mathbf{V}_A - \mathbf{L}\mathbf{M}^{-1}\mathbf{L}^T\mathbf{V}_A \\ &= (\mathbf{K} - \mathbf{L}\mathbf{M}^{-1}\mathbf{L}^T)\mathbf{V}_A\end{aligned}$$

Thus, the new reduced admittance matrix, relating $\mathbf{V}_A$ to $\mathbf{I_A}$ can be expressed as

$$\mathbf{Y} = \mathbf{K} - \mathbf{L}\mathbf{M}^{-1}\mathbf{L}^T. \tag{2.4}$$

This procedure is known as Kron reduction. If we were to apply Kron reduction, one node at a time, we could rewrite Eq. (2.4) as

$$Y_{jk(\text{new})} = Y_{jk(\text{old})} - \frac{Y_{jn}Y_{nk}}{Y_{nn}}. \tag{2.5}$$

Here is an example of Kron reduction being applied to an admittance matrix.

Example

Note that in this example, the diagonals are printed in red for the sake of legibility. Consider the following admittance 4×4 admittance matrix:

$$\begin{bmatrix} -i9.8 & 0.0 & i4.0 & i5.0 \\ 0.0 & -i8.3 & i2.5 & i5.0 \\ i4.0 & i2.5 & -i14.5 & i8.0 \\ i5.0 & i5.0 & i8.0 & -i18.0 \end{bmatrix}$$

Applying Eq. (2.5) to every every entry of the above matrix will remove the fourth node, yielding the following matrix:

$$\begin{bmatrix} -i8.4111 & i1.3889 & i6.2222 \\ i1.3889 & -i6.9111 & i4.7222 \\ i6.2222 & i4.7222 & -i10.9444 \end{bmatrix}$$

If we were to reapply this procedure so that we remove the third node, we are left with

$$\begin{bmatrix} -i4.8736 & i4.0736 \\ i4.0736 & -i4.8736 \end{bmatrix}.$$

In the above example, we reduced a four-node network to a two-node network. In their 2018 [32] and 2021 [33] papers on power grids, Arinushkin et al. applied Kron reduction to admittance matrices using MATPOWER [84] to reduce the number of equations in the systems that had to be solved. We cover their work in the following two chapters.

2.2.4 On Kron Reduction and Frustration

We denote the phase of the admittance between nodes j and k with α_{jk} such that

$$Y_{jk} = |Y_{jk}|e^{\mathbf{i}\alpha_{jk}}.$$

The frustration between nodes j and k is given by

$$\gamma_{jk} = \alpha_{jk} - \frac{\pi}{2}$$

where γ_{jk} corresponds to the frustration elements. [30] If we incorporate this frustration term into the Kuramoto model with inertia (Eq. (1.1)) in the same way as we introduced frustration in Eq. (1.3), we have

$$m_j\ddot{\theta}_j + D_j\dot{\theta}_j = \omega_j - \sum_{k=1}^{N} K_{jk}\sin(\theta_j - \theta_k - \gamma_{jk}). \tag{2.6}$$

In Eq. 2.6, we rearranged the signs to match the equations in the papers discussed in Chapters 3 and 4 [32, 33]. Note that we use a non-uniform coupling strength K_{jk} between the jth and the kth oscillators.

Frustration is related to the phase of the admittances between the generators and/or consumers in a network. In 2015, Nishikawa [30] argued that since the imaginary parts of the admittances are "mostly positive and much larger than the real parts" (which corresponds to a phase-lag of $\gamma_{ij} \approx 0$), frustration can be ignored.

However, we argue that given even a small real part for the admittance, the phase-lags in a network may become significant once Kron reduction has been applied. For example, consider the following admittance matrix where there is a non-zero real part in the admittance between the first and the third oscillator.

$$\begin{bmatrix} -i8.4111 & i1.3889 & 0.1 + i6.2222 \\ i1.3889 & -i6.9111 & i4.7222 \\ 0.1 + i6.2222 & i4.7222 & -i10.9444 \end{bmatrix}$$

We then apply Kron reduction.

$$\begin{bmatrix} 0.1137 - i4.8745 & 0.0431 + i4.07359 \\ 0.0431 + i4.07359 & -i4.8736 \end{bmatrix}$$

In this particular case, eliminating the third node changed the phase of the admittance between the first and second node from $\alpha_{12} = \frac{\pi}{2}$ to $\alpha_{12} = 1.56022$. This corresponds to the frustration changing from $\gamma_{12} = 0$ to $\gamma_{12} = -0.0105763$.

If one were to eliminate several nodes with non-zero real parts in their admittances, it could lead to the reduced matrix having quite large real parts, leading to non-trivial levels of frustration in the network.

The justification for applying Kron Reduction is that it saves time by reducing the number of nodes in a network, since the simulation time scales quadratically with the number of nodes. The non-trivial frustration elements that appear in the model as a result of the Kron reduction do not significantly increase the simulation time.

2.2.5 Computational Methods

Integrating over large systems usually requires a lot of time and computational power. In order to make such simulations faster and less computationally expensive, one typically employs some sort of optimisation method. For example, one could use some kind of precompiled library for frequently run functions in a Python script. One such example can be seen in a 2023 paper by Botha et al. [25], where they used the Dormand-Prince routine dopri5 made available through the Python module scipy.integrate. Scipy (scipy.org) is a library built on top of Python's core numerical library Numpy (numpy.org), which is used for array-manipulation and linear algebra.

Alternatively, one could use the open-source just-in-time (JIT) Python compiler NUMBA (numba.pydata.org), as we did in our work. NUMBA translates a subset of Python and NumPy code into machine code. This allows one to achieve a similar level of performance to that of lower level languages like C or Fortran, without the need to switch to another language. In addition to its use in research, NUMBA has been shown to have applications for small hardware devices. For example, in 2024, Clemente-López et al. [85] found that NUMBA could be used to speed up the code execution of encryption schemes running on IoT devices.

Chapter 3

Critique of the 2018 paper by Arinushkin and Anishchenko

The first step to modelling power grids is developing codes that solve the governing equations accurately and in a reasonable amount of time. This becomes especially challenging upon adding frustration to a model. Few publications have addressed the effects of frustration in power networks [25, 32, 33]. In this chapter, we critique one such paper by Arinushkin and Anishchenko [32]. They derived what is referred to as an effective model (EN) by reducing a larger network through Kron reduction. As Nishikawa and Motter [30] describe in a 2015 paper, an effective network consists only of generator nodes, whilst the loads are modelled as constant impedences. In the paper by Arinushkin and Anishchenko, the network consists of only three generators.

In order to test our codes, we tried to replicate their plots. We used RK45 from the scipy.integrate Python sub-package as our numerical integration method. However, we could not reproduce their results. We identify the problems with their work. In particular, we point out that the numerical noise in their plots is due to their use of too large a time-step. They used the following Kuramoto-like equation to model the system:

$$\frac{2H_i}{\omega_R}\ddot{\delta}_i + \frac{D_i}{\omega_R}\dot{\delta}_i = A_i^{\mathrm{EN}} - \sum_{j=1, j\neq i}^{n_g} K_{ij}^{\mathrm{EN}} \sin(\delta_i - \delta_j - \gamma_{ij}^{\mathrm{EN}}) \tag{3.1}$$

The parameter values were defined as follows (see Fig. 3.1 for reference):

A_i^{EN} is related to the power generated by the ith oscillator.

H_i is the inertia of the ith oscillator.

D_i is the damping term for the ith oscillator.

ω_R is the reference frequency of the system (in rad/s).

K_{ij}^{EN} is the coupling strength between the ith and the jth oscillator.

γ_{ij} is the frustration in the coupling between the ith and the jth oscillator.

δ_i is the oscillator's phase relative to the synchronous axis.

To clarify, A_i^{EN} is not *directly* proportional to the power generated by the ith generator, $P_{g,i}$. Rather, it is related to $P_{g,i}$ by the equation $A_i^{\text{EN}} = P_{g,i} - |E_i|^2 G_{ii}^{\text{EN}}$, where E_i is the voltage of the ith generator in the reduced network, and G_{ii}^{EN} is the real part of the admittance Y_{ii}^{EN} [30]. The term $-|E_i|^2 G_{ii}^{\text{EN}}$ accounts for the omitted term in the summation, where $i = j$.

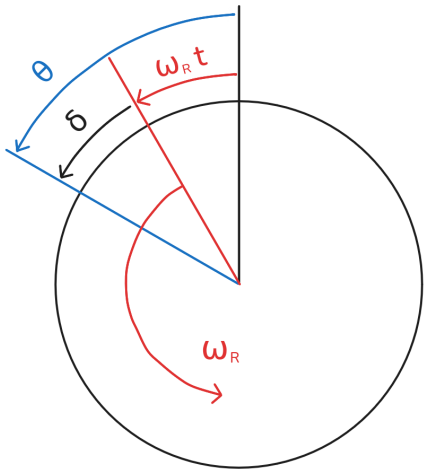

Figure 3.1: $\omega_R t$ is the phase of the synchronously rotating axis (red) relative to the reference axis (black). θ is the phase of the oscillator (blue) relative to the reference axis (black). δ is the oscillator's (blue) phase relative to the synchronous axis. (red)

In Ref. [32], the inertia, coupling strengths, levels of frustration, and power generated differed for each oscillator. We constructed a similar system with slightly different parameter values to test whether we could replicate their findings. The parameter values for the system were $A_1 = -0.2276$, $A_2 = 2.2349995$, $A_3 = 0.5635$, $H_1 = 23.64$, $H_2 = 6.4$, $H_3 = 3.01$, $D_i = 50$, $\omega_R = 314.1593$, $K_{12} = 1.7089$, $K_{13} = 1.3361$, $K_{23} = 1.184$,

$\gamma_{12} = -0.1875$, $\gamma_{13} = -0.1694$, and $\gamma_{23} = -0.1964$. In addition, we use X_i to denote the initial phase of the *ith* oscillator. In their case, they let $X_2 = 2.0944$ and $X_3 = 4.1889$. X_1 is varied for the figures.

They rewrote Eq. (3.1) as the system of equations:

$$\dot{x_i} = y_i$$
$$\dot{y_i} = \Big(A_i - \sum_{j=1, j\neq i}^{n_g} K_{ij} \sin(x_i - x_j - \gamma) - \frac{D_i}{\omega_R} y_i\Big) \frac{\omega_R}{2H}$$

Here they replaced δ_i and $\dot{\delta}_i$ with x_i and y_i respectively, and omitted the EN superscripts.

3.1 Evolution of phase velocities and the importance of an appropriate time step size

In their paper [32], Arinushkin and Anishchenko used a time step size of 0.2. Using a time step of 0.2 in our system, where $X_1 = 0$, as seen in Fig. 3.2 (a), yields a plot in which the system synchronises. Using an adaptive time step that reduces the time step size until some error tolerance is met, as seen in Fig. 3.2 (e), yields a plot in which the system remains asynchronous. This demonstrates the importance of using an appropriate time step size when plotting the evolution of the system. Furthermore, this calls into question the validity of their results.

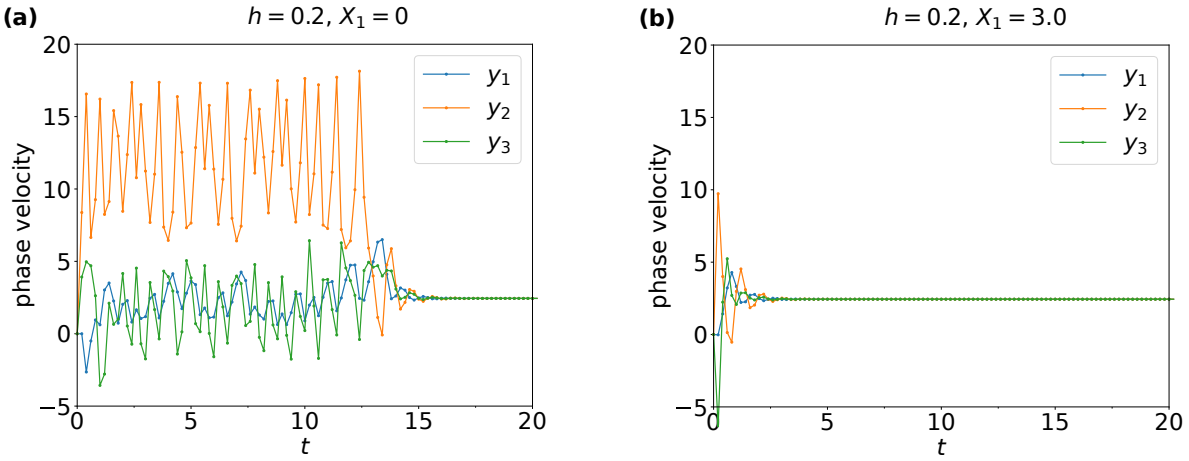

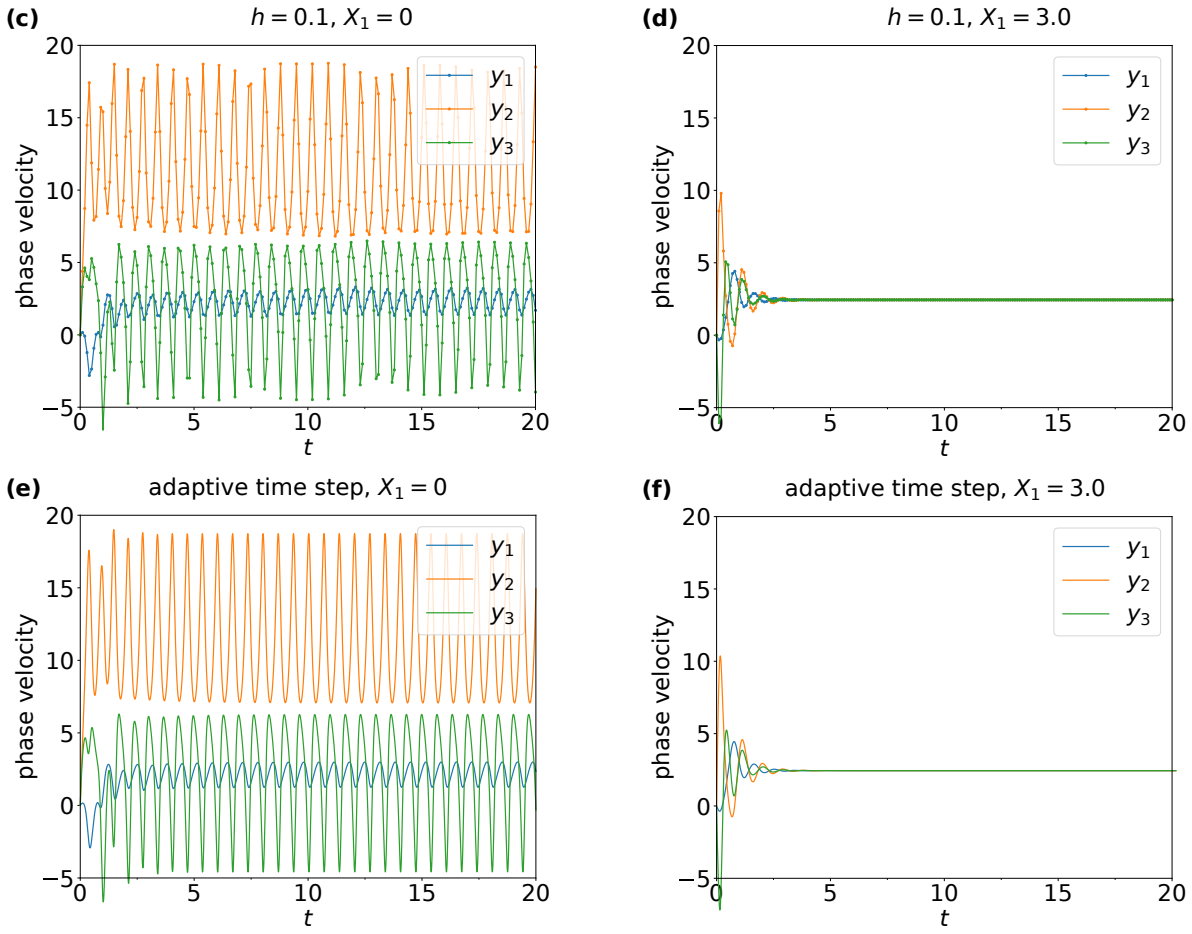

Figure 3.2: Plots of phase velocities over time for different time step sizes and initial conditions. The bottom two figures refer to the cases where an adaptive time step is used with an absolute and relative error tolerance of 1.0×10^{-13}. (a) $X_1 = 0$, $h = 0.2$. (b) $X_1 = 3.0$, $h = 0.2$. (c) $X_1 = 0$, $h = 0.1$. (d) $X_1 = 3.0$, $h = 0.1$. (e) $X_1 = 0$. Adaptive time step. (f) $X_1 = 3.0$. Adaptive time step.

3.2 Basins of stability

In the following figures, we plot the regions for which the system synchronises. Whenever the time to synchronise exceeds the transient time of 200 time units, we consider the system to be asynchronous.

3.2.1 Effects of initial conditions on synchronisation

According to Ref. [32], the system is sensitive to changes in the initial conditions, i.e. the initial phases of the oscillators. In Fig. 3.3, we plot the regions for which the system

synchronises over ranges of the phases of the first and second oscillators. The parameter values are the same as for Fig. 3.2, except that $A_2 = 1.1668$. This makes the parameter values for Fig. 3.3 identical to that of one of the systems that they tested (Fig. 4 in the original paper).

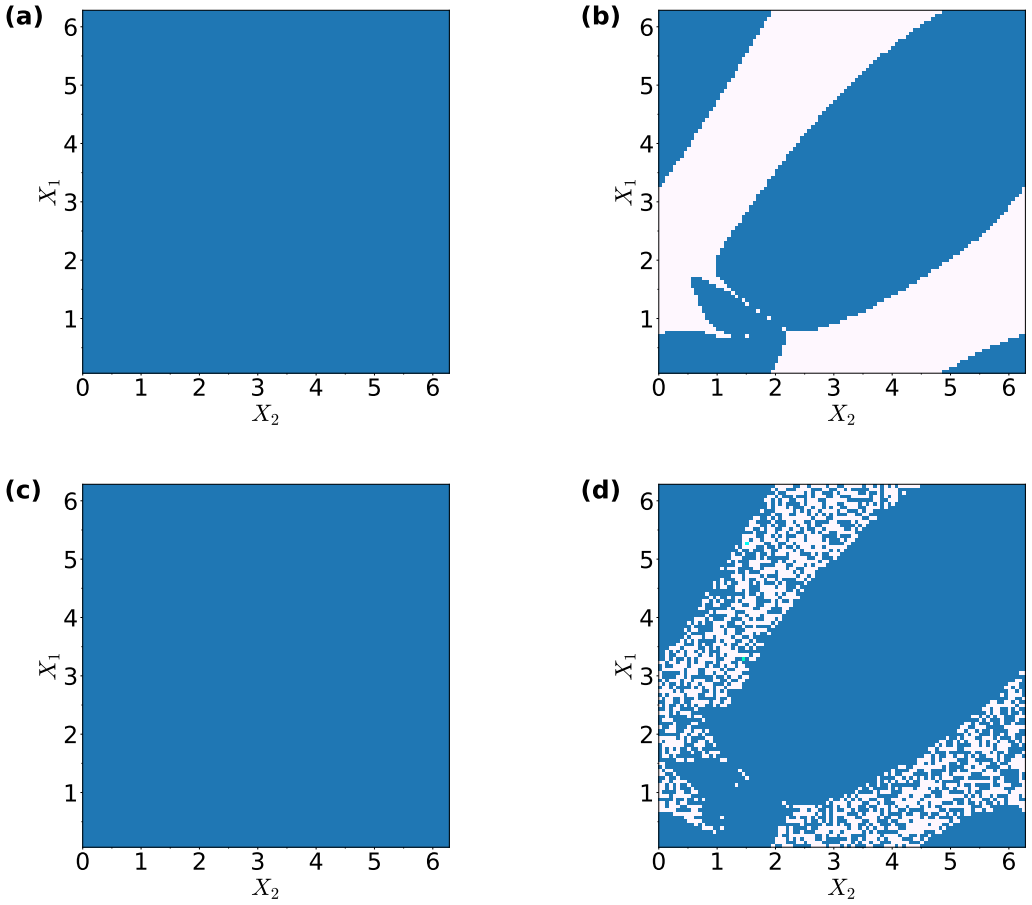

Figure 3.3: Maps of the synchronous (blue) and asynchronous (white) regions for the system over the phases X_1 and X_2. X_3 is set to 0. We vary the damping D_i and the timestep h for each plot. (a) $D_i = 50$. Adaptive timestep. (b) $D_i = 10$. Adaptive time step. (c) $D_i = 50$. $h = 0.2$. (d) $D_i = 10$. $h = 0.2$.

The parameter values for the system in Fig. 3.4 are $A_1 = -0.2276$, $A_2 = 1.7238$, $A_3 = 0.5635$, $H_1 = 23.64$, $H_2 = 6.4$, $H_3 = 3.01$, $D_i = 50$, $\omega_R = 314.1593$, $K_{12} = 1.7274$, $K_{13} = 1.333$, $K_{23} = 1.1982$, $\gamma_{12} = -0.1912$, $\gamma_{13} = -0.1726$, and $\gamma_{23} = -0.1959$. These match the parameter values of another system that they tested (Fig. 5 in the original paper).

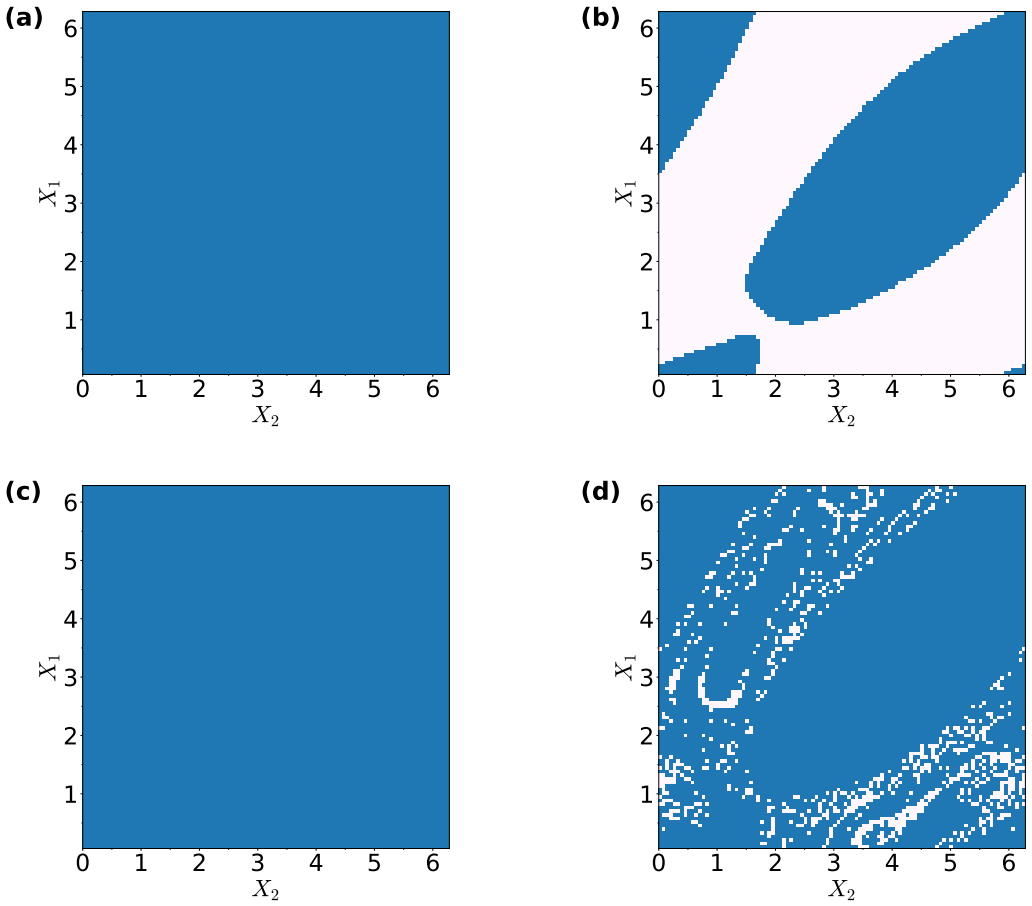

Figure 3.4: Maps of the synchronous (blue) and asynchronous (white) regions for the system over the phases X_1 and X_2. X_3 is set to 0. We vary the damping D_i and the timestep h for each plot. (a) $D_i = 50$. Adaptive timestep. (b) $D_i = 10$. Adaptive time step. (c) $D_i = 50$. $h = 0.2$. (d) $D_i = 10$. $h = 0.2$.

These plots confirm that whether or not a system synchronises depends partially on its initial conditions. We found that, whenever the system does synchronise, the time to synchronise is roughly inversely proportional to the damping constant, ranging from 20 timesteps when the damping constant is set to 50, to 120 timesteps for a damping constant of 10. Note that it is unnecessary to vary X_3. This is evident when we observe that

$$\begin{aligned}
\dot{y_i} &= \Big(A_i - \sum_{j=1,j\neq i}^{n_g} K_{ij}\sin(x_i - x_j - \gamma) - \frac{D_i}{\omega_R}y_i\Big)\frac{\omega_R}{2H} \\
&= \Big(A_i - \sum_{j=1,j\neq i}^{n_g} K_{ij}\sin(x_i + \alpha - x_j - \alpha - \gamma) - \frac{D_i}{\omega_R}y_i\Big)\frac{\omega_R}{2H} \\
&= \Big(A_i - \sum_{j=1,j\neq i}^{n_g} K_{ij}\sin((x_i + \alpha) - (x_j + \alpha) - \gamma) - \frac{D_i}{\omega_R}y_i\Big)\frac{\omega_R}{2H}
\end{aligned}$$

This proves that if we were to increase every phase x_i in the system by the same amount α, $\dot{y_i}$ would remain unchanged. Similarly, $\dot{x_i}$ would be unaffected since we did not alter the phase velocities y_i. Thus, the evolution of the whole system remains unaffected if we offset all the initial phases by the same amount.

Consider a system with initial phases (x_1, x_2, x_3). Suppose x_3 is increased by α. The initial phases would then be $(x_1, x_2, x_3 + \alpha)$. We can decrease all three phases by α without any change in the behaviour of the system. Thus

$$(x_1, x_2, x_3 + \alpha) = (x_1 - \alpha, x_2 - \alpha, x_3 + \alpha - \alpha) = (x_1 - \alpha, x_2 - \alpha, x_3)$$

Therefore, varying X_3 is unnecessary in Fig. 3.3 and Fig. 3.4.

3.2.2 Differentiating between quasi-periodicity and chaos

We also differentiated between the chaotic and quasi-periodic states of the system by analysing its Lyapunov exponents. To calculate the Lyapunov exponents, we use the standard WSSV algorithm [86]. For this purpose, we again used RK4 with the adaptive time stepping. By combining this data with plots generated for the periodicity of synchronous states we can construct a plot where the synchronous, quasi-periodic, and chaotic regions of the system are visible.

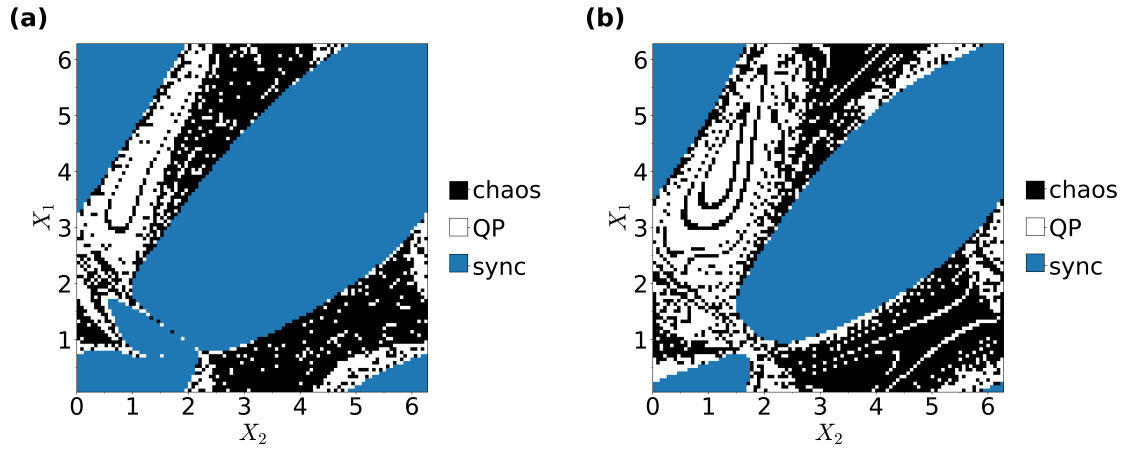

Figure 3.5: Maps of the synchronous (sync), quasi-periodic (QP), and chaotic (chaos) regions for the system over the phases X_1 and X_2. X_3 is set to 0. (a) The parameters correspond to the system for Fig. 3.3. (b) The parameters correspond to the system for Fig. 3.4.

3.2.3 Discussion

In their paper, Arinushkin and Anishchenko [32] attempted to test whether the initial phases of the oscillators determined whether or not their three-generator network synchronises. Their plots indicated that the initial conditions do in fact play a role in the synchronicity of the the network. However, in our attempt to replicate their results, we found problems in their work. For example, the plots of Fig. 4 in their paper, which corresponds to the system described in Fig. 3.3, indicate that the synchronicity of the system with the damping set to $D_i = 50$ is sensitive to initial conditions. Our plots in Fig. 3.3 (a) and Fig. 3.3 (b) show this not to be the case. Furthermore, the time-step of $h = 0.2$ that they used was too large, as can be seen when we compare the noisy plot for the fixed time-step of $h = 0.2$ in Fig. 3.3 (b), with the plot for a dynamic time step in Fig. 3.3 (d).

We repeated similar tests in Fig. 3.4, corresponding to Fig. 5 in their paper. These plots indicate the same flaws as mentioned above. This highlights the importance of choosing an appropriate time-step size when simulating continuous dynamical systems.

Chapter 4

Evaluation of proportional and nonlinear damping control schemes in an optimised power grid

4.1 Introduction

One of the key requirements to avoid cascading failures, i.e. blackouts, in power transmission grids, is their ability to operate stably in a synchronous mode [1, 52, 87]. In recent times, however, growing demands made on existing power grids, such as, increasing loads and pressure to incorporate more environmentally-friendly energy sources, like wind and solar [22], have threatened to collapse entire grids. In South Africa, for example, in order to avoid a complete collapse, very high levels of so-called "load shedding" have had to be implemented, at a huge cost to the economy [88]. In this context, the study of electrical power grids, with the view of developing better future grids (as discussed in [89], for example), is a national priority, if not a priority for mankind in general.

In an attempt to improve the stability of synchrony in smart grids, several studies have attempted to incorporate different forms of control. Following the detailed approach, Singh and Pak [90] have proposed a decentralised method for nonlinear control of oscillatory dynamics in power systems. Their method ensures that there is both transient stability and small-signal stability in the network by using an optimal control law, derived within the general framework of nonlinear control by using normal

forms. Taher et al. [91] have also suggested the use of time-delayed feedback control, to improve stability. Recently, Arinushkin and Vadivasova [33] have demonstrated that nonlinear damping can prevent the asynchronous behaviour of oscillators and increase the stability of the grid with respect to intermittent fluctuations. They made use of an optimised model in which the consumer dynamics have been eliminated from consideration, thereby reducing the total number of equations required to describe the power grid [30]. In this model, the nonlinear coupling results in a dependency between the power of the rotors, and the natural frequency with which they tend to rotate; in much the same way as the frequency of a simple pendulum becomes dependent on its amplitude, for large angle (nonlinear) oscillations. The nonlinearity in the damping coefficient was introduced in such a way that the energy damping in each oscillator depended on its rotation frequency. Such a control scheme; however, had a strong dissipative effect on the connected power rotors, which could lead to overheating and failure [33].

In what follows, we apply a proportional control scheme that was successfully used by Sieber et al. [92] to stabilise chimera states in a system governed by, essentially, the Kuramoto-Sakaguchi model without any inertial terms. We will show that this form of reactive power control [93] is also able to stabilise a power grid and that it may offer some advantages in comparison to the nonlinear damping control method described in [33].

4.2 Model and Methods

We consider the model presented in [33], for which the dynamical equations for δ_j (the phase of each rotor relative to the reference phase, $\omega_R t$), are given by

$$\frac{2H_j}{\omega_R}\ddot{\delta}_j + \frac{D_j}{\omega_R}\dot{\delta}_j = A_j - \sum_{\ell=1,\ell\neq j}^{n_g} K_{j\ell}\sin(\delta_j - \delta_\ell - \gamma_{j\ell}) \tag{4.1}$$

where H_j and D_j represent the inertia and damping of the jth oscillator, respectively. In this model, A_j is the rotor power output and the matrices $K_{j\ell}$ and $\gamma_{j\ell}$ set the strength and phase shift of the coupling between rotors j and ℓ, respectively. The actual instantaneous frequency of each rotor is given by the formula $f_j = 0.5(\dot{\delta}_j + \omega_R)/\pi$. We make use of the numerical values for the A_j, $K_{j\ell}$ and $\gamma_{j\ell}$, given in Tables 3-5 of [33], for $n_g = 10$. In [33] the inertia coefficients $H_j = H$ were assumed to be equal, allowing H to be used as one of two control parameters; the other being the power generated by the 5th oscillator, $P_{g,5}$. Here, for the purpose of comparison, we do the same.

Instead of exercising control on the system through the addition of nonlinear damping to *all* ten rotors, i.e. via $D_j = D_{0j} + k|\dot{\delta}_j|$, as given by Eq. (9) of [33], we apply a proportional control scheme similar to that used in [92] to try to stabilise the synchronous state of the system. In our case, we apply the control law,

$$D_5 = D_0 - \eta\,[r(t) - r_0]\,, \tag{4.2}$$

only to the 5th rotor. Here, $D_0 = D_{0j} = 50$ is the constant component of the damping coefficient (assumed, as in [33], to be the same for all the rotors), $r(t) = n_g^{-1}|\sum_{k=1}^{n_g} e^{i\delta_k(t)}|$ is the global order parameter ($r(t) = r_0 = 1$ for full synchronisation), and η is the damping control gain parameter [92].

Additionally, we investigate the effect of controlling the phase-lags relative to the 5th rotor, according to the proportional control law,

$$\gamma_{5\ell} = \gamma_{0\,5\ell} - \xi(r(t) - r_0). \tag{4.3}$$

Here, the symbols $\gamma_{0\,5,\ell} = \gamma_{0\,\ell,5}$ refer to the original values specified in the Table 5 of [33] and ξ is the phase-lag control gain parameter. In [92] a similar control scheme was used to stabilise chimera states in the Kuramoto-Sakaguchi model without the inertial terms, i.e. the terms proportional to H_j in Eq. (4.1). For a chimera state to exist, all the oscillators in the system must be identical. For that reason, the unperturbed phase-lags considered in [92] were all equal and the same form of control law, as given by Eqs.(4.2) or (4.3) (cf. Eq. (6) of [92]), was applied to *all* the oscillators.

To investigate the effects of Eqs. (4.2) and (4.3) on the different possible synchronisation regimes of the system (4.1), we followed the same methodology described in [33]. For each pair of control parameters $(H, P_{g,5})$ we evolved the system for 200 time units, starting from the same 15 randomly chosen initial conditions in the range $\delta \in [-\pi, \pi]$ and $\dot{\delta} \in [-100, 100]$. For convenience we parameterised the values of A_j linearly, according to the values given in Table 3 of [33], as $A_j = 0.009827 P_{g,j} - 0.65251$. At the end of the time integration, we recorded the three possible regimes: **1**. – if the system synchronised for all 15 initial conditions, i.e. $\langle\dot{\delta}_j\rangle_t = \text{constant}$, $\forall j = 1, 2, \ldots, n_g$. **2**. – if the system was bi-stable in that it only synchronised for some of the initial conditions. **3**. – if the system did not synchronise for any of the initial conditions.

As a tolerance for detecting the frequency synchronisation regime **1**, we used $\sigma < 10^{-13}$, where σ is the standard deviation of the set of time averaged frequencies: $\{\langle\dot{\delta}_j\rangle_t \,|\, j = 1, 2, \ldots, n_g\}$. To compute the time averages, $\langle\dot{\delta}_j\rangle_t$, we sampled the last 100 time units of the system's trajectory, at fixed intervals of 0.2 time units.

Because the system of Eqs. (4.1) was found to be stiff in some cases, we used the `lsoda` method provided by Python's `ode` interface from the sub-package `scipy.integrate` to obtain the systems time evolution [94]. This method switches automatically between the implicit Adams method (for non-stiff problems) and a method based on backward differentiation formulas for stiff problems. We set the relative and absolute integration error tolerances in `lsoda` to 10^{-12}.

4.3 Results

We first apply the proportional control scheme via the damping constant of the 5th rotor, as given by Eq. (4.2). Fig. 4.1 shows

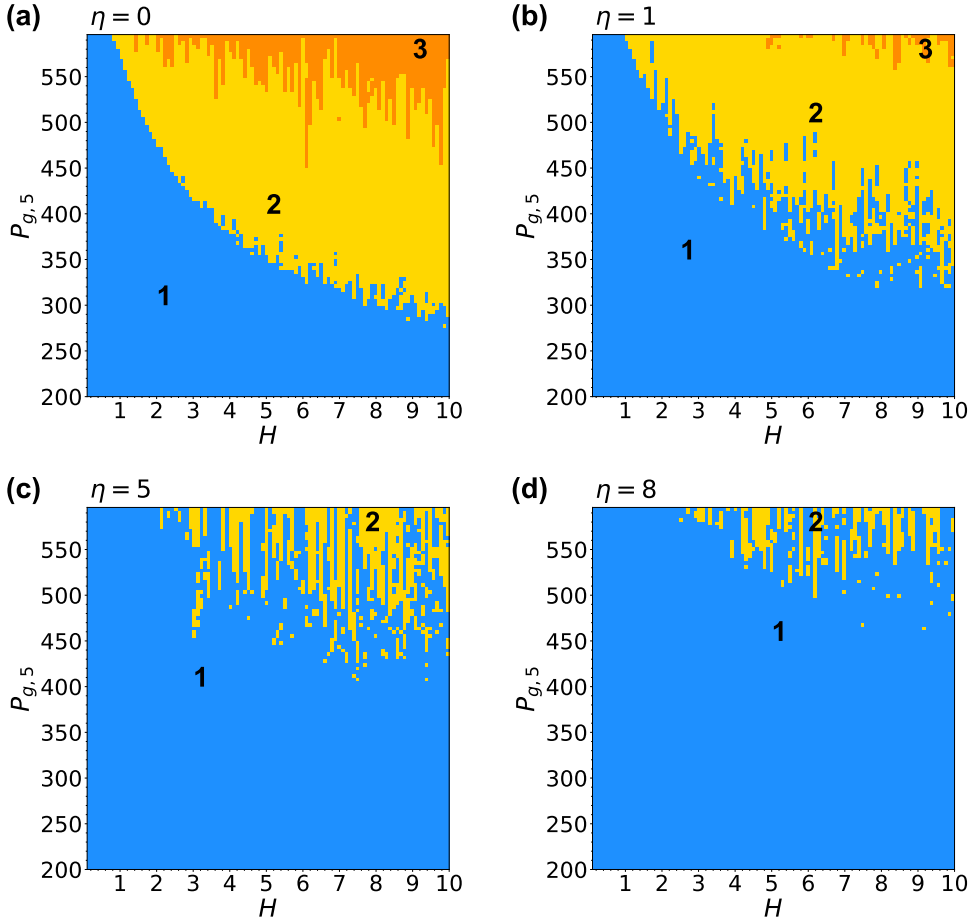

Figure 4.1: Regime maps of the network of nonlinear oscillators discussed in [33], showing the effect of increasing η in the proportional control effected by Eq. (4.2), on synchronicity within the grid at (a) $\eta = 0$ (no control), (b) $\eta = 1$, (c) $\eta = 5$ and (d) $\eta = 8$. Here the control parameters are the inertia parameter H and the output power of the 5th rotor $P_{g,5}$, with: 1 - area of the synchronous mode (blue); 2 - area of bi-stability (yellow); 3 - area of asynchronous behaviour of one or more oscillators (orange).

the effect of increasing the control gain parameter, η, on the synchronisation regimes occurring withing the 2-dimensional control parameter space. Fig. 4.1 (a) corresponds to the case of no control, and is qualitatively the same as Fig. 1 of [33]. A comparison of Figs. 4.1 (a)-(d) shows that the region of synchronisation (**1**–blue) expands significantly with increasing η. The region corresponding to the asynchronous mode (**3**-orange) shrinks rapidly with increasing η, as can be seen in Fig. 4.1 (b), and in fact completely disappears for $\eta \gtrapprox 1$ (not shown). For $\eta = 5$, as seen in Fig. 4.1 (c) the remaining bi-stable region (**2**-yellow) has shrunk further and become more fragmented, being interspersed with many small areas of synchronous behaviour. This trend continues as η increases further to $\eta = 8$, as see in Fig. 4.1 (d), until the whole region become completely synchronous for $\eta \gtrapprox 10$ (not shown). The results of Fig. 4.1 may be easily compared to those of [33] and such a comparison shows that the proportional control scheme given by Eq. (4.2) is equally effective as applying nonlinear damping control to all the rotors.

The main advantage of Eq. (4.2) is that it only acts on one of the rotors, which means that it introduces far less dissipation into the system than the nonlinear damping scheme of [33].

In Fig. 4.2 we again investigate the effect of applying proportional control via Eq. (4.2), but this time we look in detail at the time dependence of the phases δ_j, as the system evolves from one specific initial condition, chosen from the random set of 15 that was used previously. (See, Sec. 4.2.) The modulo of the phases, shifted to lie between $-\pi$ and π, is represented by the range of colours indicated along the colour bars in Fig. 4.2 (the same for all figures). If the oscillators were fully synchronised, we would see the same repeating phase for each oscillator, forming a repeating series of different colours aligned horizontally, with time increasing in the vertical direction. Phase synchronous behaviour (which implies frequency synchronisation, i.e. $\langle \dot{\delta}_j \rangle_t =$ constant) shows up in these figures as fixed shifts between the sequences of colours representing phases of each rotor, labelled 1 to 10 on the horizontal axes. In Fig. 4.2 (a) we see the case of no control, corresponding to the (yellow) point $(H, P_{g,5}) = (5, 400)$ in Fig. 4.1 (a). In this specific case the system does not synchronise and the higher frequency is maintained by the 5th rotor, in comparison to all the other rotors, for which $P_{g,j} = 200\,(j \neq 5)$. We see also that the slower group of rotors do behave coherently, in that they reach a state in which their time averaged frequencies are practically the same, giving the appearance of phase synchronisation. When control is applied at the level of $\eta = 1$, as show in Fig. 4.2 (b), the higher frequency of the 5th rotor is rapidly pulled down towards that of the others, and the system as a whole becomes synchronised, within 1-2 seconds. Although one cannot conclude it by merely looking

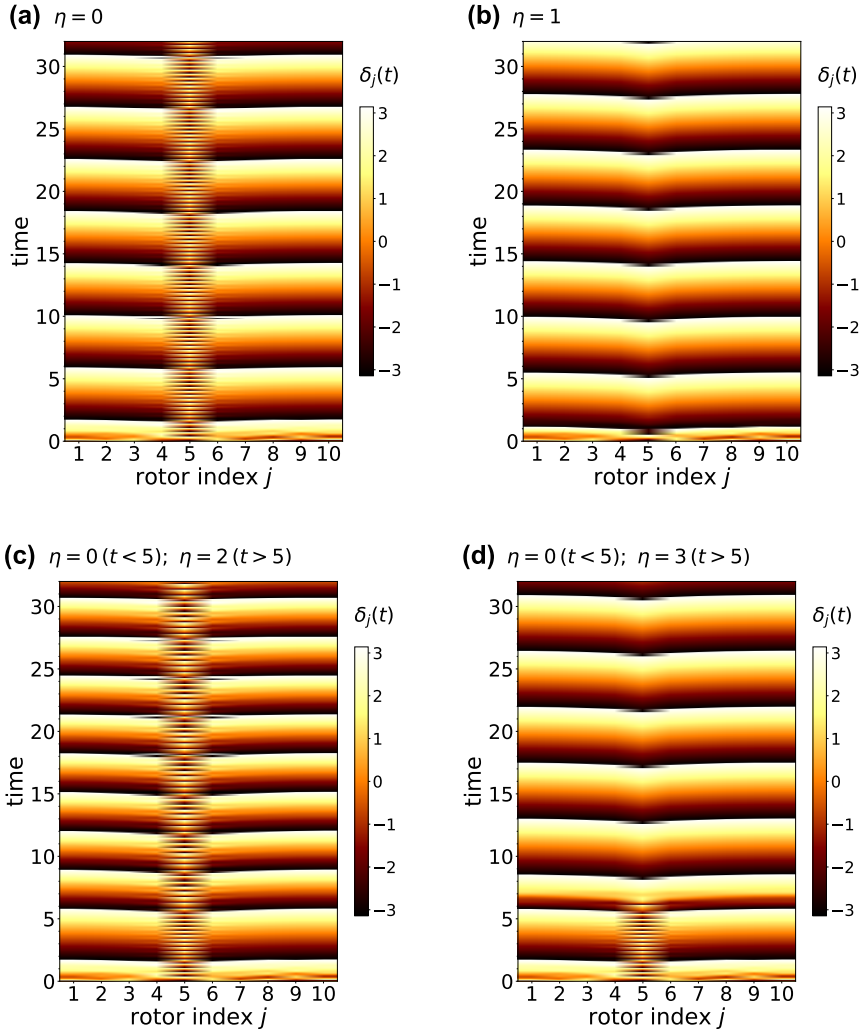

Figure 4.2: The time evolution of the instantaneous phases $\delta_j(t)$ for $j = 1, 2, \ldots, n_g$. The colour scale indicates the mod of each phase, between $-\pi$ and π. In (a), no control is exercised ($\eta = 0$) and consequently the 5th rotor, for which $P_{g,5} = 400$ does not synchronise with the others, for which $P_{g,j} = 200$, $j \neq 5$. In (b), the damping control gain parameter for the 5th oscillator is set to $\eta = 1$ at $t = 0$, causing the system to synchronise after a short transient time (approximately 1 to 2 seconds). In (c), no control is exercised for the first 5 seconds of the simulation; thereafter $\eta = 2$ is implemented, but the system does not synchronise, even after a long time. In (d), $\eta = 3$ control is implemented after the first five seconds (as in c), but this time the larger control gain does bring about synchronisation after a short transient time (approximately 2 to 3 seconds). These behaviours are discussed in more detail in the main text. Other parameters are: $n_g = 10$, $H = H_j = 5$ for $j = 1, 2, \ldots, n_g$, $D_0 = 50$, and $\omega_R = 2\pi \times 50$.

at Fig. 4.2 (b), an analysis of the data for this figure shows that the system is in fact also phase synchronised.

We have also tested the effect of applying the control after the system has evolved for different times. For such cases the control is not as effective as when it is applied right from the outset, at $t = 0$. In Fig. 4.2 (c) we see, for example, a case when no control was exercised over the first 5 seconds. Thereafter, the control gain parameter was set to $\eta = 2$, which is twice the value used in (b), using the same initial condition. Despite the larger value of η, the delay in the application of the control causes the system not to become synchronised. This behaviour may be attributed to the onset of coherence among the other oscillators ($j \neq 5$), which tends to push up the value of $r(t)$ for the system, closer to $r_0 = 1$, thereby effectively reducing the amplitude of the proportional control. To confirm this hypothesis, we performed the same experiment as in (c), with systematically increasing values of η. By the time η reached approximately 3, the delayed application of the control was indeed successful in synchronising the network, as shown in Fig. 4.2 (d).

We can see the difference between Fig. 4.2 (c) and (d) in more detail by examining the time dependence of the order parameter and the time averages of the rotors, as is shown in Fig. 4.3. In Fig. 4.2 (a) we see that, shortly before the control is switched on, the order parameter is oscillatory, and oscillating about a mean value of about 0.9, with amplitude ≈ 0.1. Since the control is proportional to $(r(t) - 1)$, the effective proportional control being applied at $t = 5$ is only about 10% of η.

This is much smaller than in the case when the control is applied at $t = 0$, before the order parameter settles down into oscillatory behaviour. Hence, in Fig. 4.3 (a) we see that, after the control has been switched on at $t = 5$, the system with the larger control ($\eta = 3$, given by the blue solid line) becomes synchronised with $r(t) = 0.9843$, while the $r(t)$ for the $\eta = 2$ system (shown by the red dashed line), continues to oscillate about $\langle r(t) \rangle_t = 0.8551$. In Fig. 4.3 (b), the time averaged frequencies are shown for the same two cases over the interval $t \in [24, 32]$. For the asynchronous regime (red squares), the final average frequency of the 5th oscillator is $(52.281 \pm 0.016)\,\mathrm{Hz}$, which is considerably lower than its natural frequency $f_5^* = 53.7728\,\mathrm{Hz}$ (calculated according to Eq. (11) of [33]). We can compare this result to the asynchronous regime, shown in Fig. 3 (b) of [33], for which the average frequency of the 5th rotor was found to be $(53.61 \pm 0.84)\,\mathrm{Hz}$. Thus, even though the proportional control does not synchronise the grid in the $\eta = 2$ case, it reduces the average frequency of the 5th rotor, significantly, and much more than in the case of nonlinear damping control applied to all the rotors.

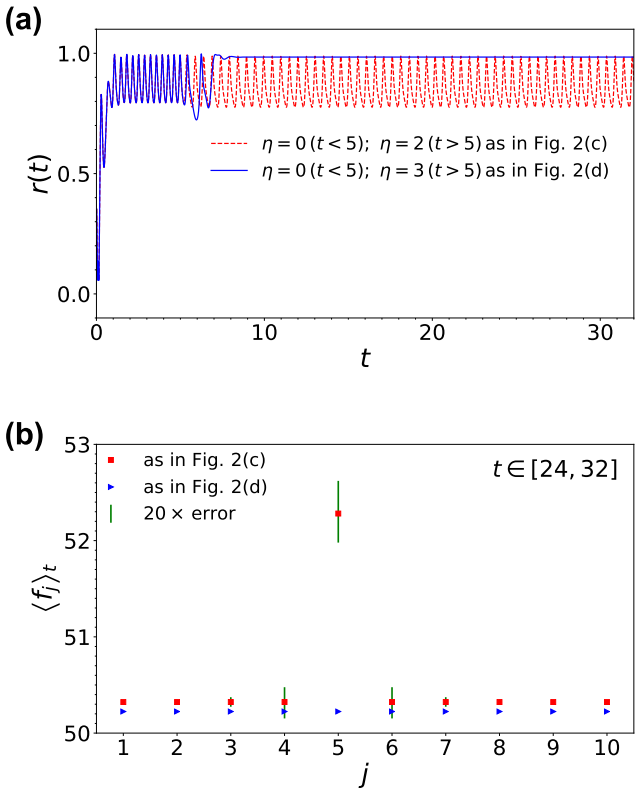

Figure 4.3: (a) Time series of the order parameter and (b) the average of the actual frequencies of the rotors for the two cases discussed previously in connection with Figs. 4.2 (c) and (d). For the case corresponding to (c) the time series is indicated by a red dashed line, while for the case corresponding to (d) it is shown by a blue solid line. Similarly, the averaged frequencies are shown by red squares in the case corresponding to (c) and by blue triangles in the (d) case. In (b), the time averages were computed over the interval $t \in [24, 32]$, using 512 samples at intervals of 1/64. The error bars in (b) show 20 times the standard deviation of the 512 samples taken for each rotor.

For the $\eta = 3$ case, where the system does synchronise, the final average frequency of the rotors is 50.224122 Hz (shown by the blue triangles), with a standard deviation of 1.1×10^{-13} Hz. This frequency is slightly closer to the reference frequency of 50 Hz, i.e. compared to the case of the nonlinear damping (50.2828 Hz) – see, Fig. 3 (a) of [33].

Another possible way of exercising control on this system is by applying the nonlinear damping control scheme of [33] *only* to the 5th oscillator. As this situation was not given much consideration in [33], we tested it here. Surprisingly, as Fig. 4.4 shows, nonlinear damping applied only to the 5th rotor, appears to be more effective than the original nonlinear damping scheme proposed in [33]. We see, in Fig. 4.4, how the synchronous regime is greatly expanded by the addition of relatively small nonlinear

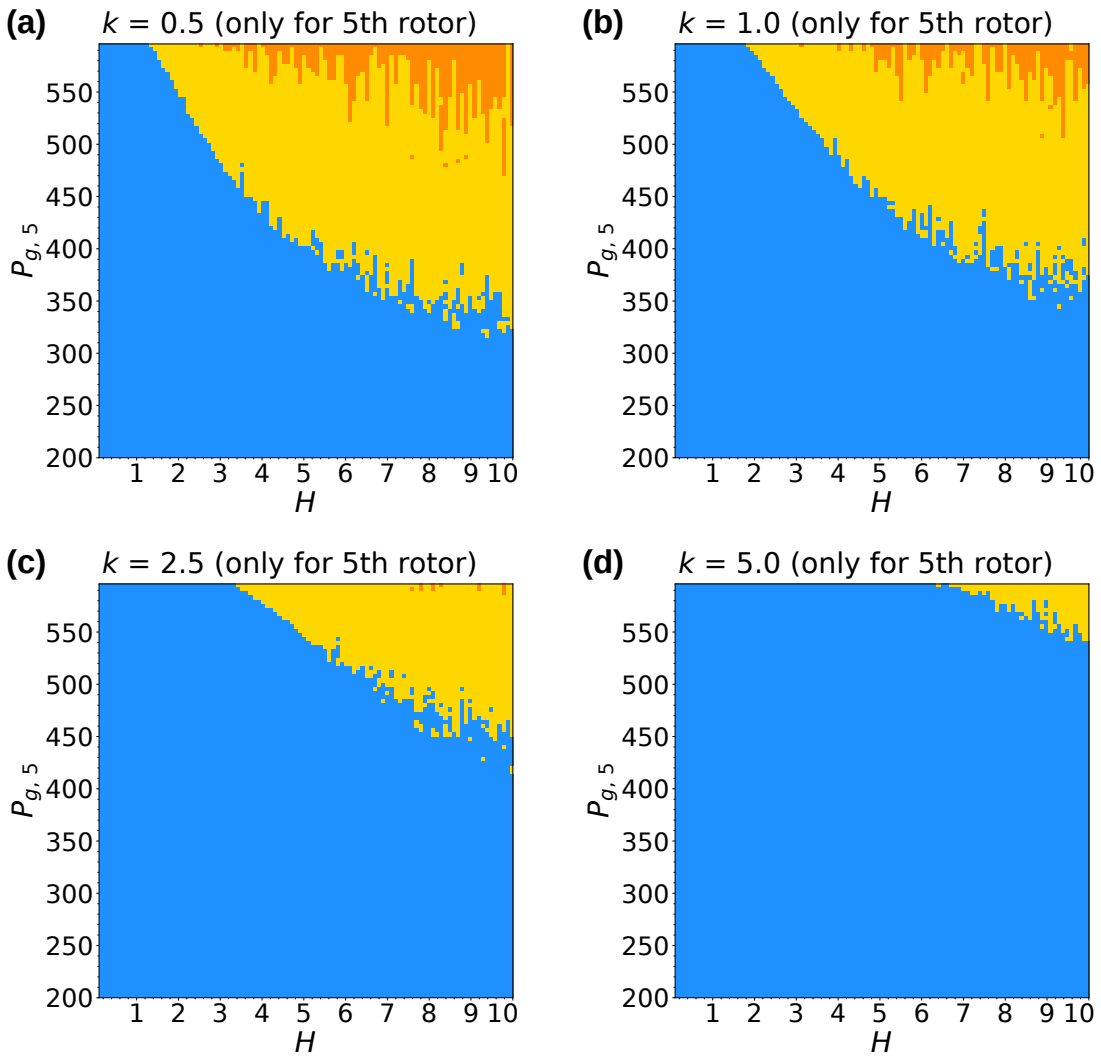

Figure 4.4: Regime maps of the network of nonlinear oscillators discussed in [33], showing the effect of increasing k when the nonlinear control scheme is applied only to the 5th rotor. (a) $k = 0.5$, (b) $k = 1.0$, (c) $k = 2.5$, (d) $k = 5.0$. The meaning of the colour scale is the same as in Fig. 4.1.

damping. If we compare the values of k used in Fig. 4 of [33] ($k = 1, 3, 5$ and 6), we see that a similar level of control is achieved by controlling only the 5th rotor.

Once the system has synchronised we can compare, for each rotor, the ratio of the average power lost due to the damping, to the rotor power output A_j. Table 4.1 shows that the added nonlinear damping in the 5th rotor consumes about 12% of its power, while the linear damping in the 5th rotor consumes 9.41% and 34% in each of the other rotors.

Table 4.1: The time average of the relative power dissipated by the 1st and 5th rotors for the case when the nonlinear damping is being applied to the fifth rotor, only.

	$j=1$	$j=5$
$\left\langle \frac{D_{0j}}{A_j\omega_R}\lvert\dot{\delta}_j\rvert \right\rangle_t$	34.0%	9.41%
$\left\langle \frac{D_{0j}+k\lvert\dot{\delta}_j\rvert}{A_j\omega_R}\lvert\dot{\delta}_j\rvert \right\rangle_t$	N.A.	12.0%

We can compare the values seen in Table 4.1 with those shown in Table 4.2, for the case where the nonlinear damping is applied to *all* the rotors in the grid. For the latter case, the added nonlinear damping in the 5th rotor consumes about 10% of its power, while the nonlinear damping to any of the other rotors consumes about 36.1% of their output power.

Table 4.2: The time average of the relative power dissipated by the 1st and 5th rotors for the case when the nonlinear damping is being applied to all the rotors.

	$j=1$	$j=5$
$\left\langle \frac{D_{0j}}{A_j\omega_R}\lvert\dot{\delta}_j\rvert \right\rangle_t$	29.1%	8.0%
$\left\langle \frac{D_{0j}+k\lvert\dot{\delta}_j\rvert}{A_j\omega_R}\lvert\dot{\delta}_j\rvert \right\rangle_t$	36.1%	10.0%

We can now compare the total power lost due to damping in each case. For the case when the nonlinear damping is applied to only the 5th rotor (Table 4.1), we have:

$$0.12A_5 + 0.34\sum_{j\neq 5} A_j = 4.57$$

For the case where nonlinear damping is applied to all the rotors (Table 4.2), we have:

$$0.10A_5 + 0.36\sum_{j\neq 5} A_j = 4.71$$

Thus, applying the nonlinear damping to only the 5th rotor results in $\approx 0.3\%$ reduction in the total dissipation. While this is not a significant reduction, it shows that the application of nonlinear damping to only the 5th rotor (an intervention that is obviously easier to implement), is not likely to increase the total dissipation in the network.

Lastly, we consider whether we may usefully apply proportional control to the phase-lags of the coupling between the 5th oscillator and the other oscillators in the network.

In principle, such a form of control would have the advantage of introducing less dissipation into the network, since the phase-lags are proportional to the complex part of the impedances (reactances) of the transmission lines joining the power rotors/consumers. The phase-lags could therefore be manipulated by adding a variable amount of capacitance to the line. Here, we will not consider the technical challenges associated with implementing a control scheme involving variable capacitance. Instead, we will merely try to establish, according to our optimised model, whether it may be worth considering.

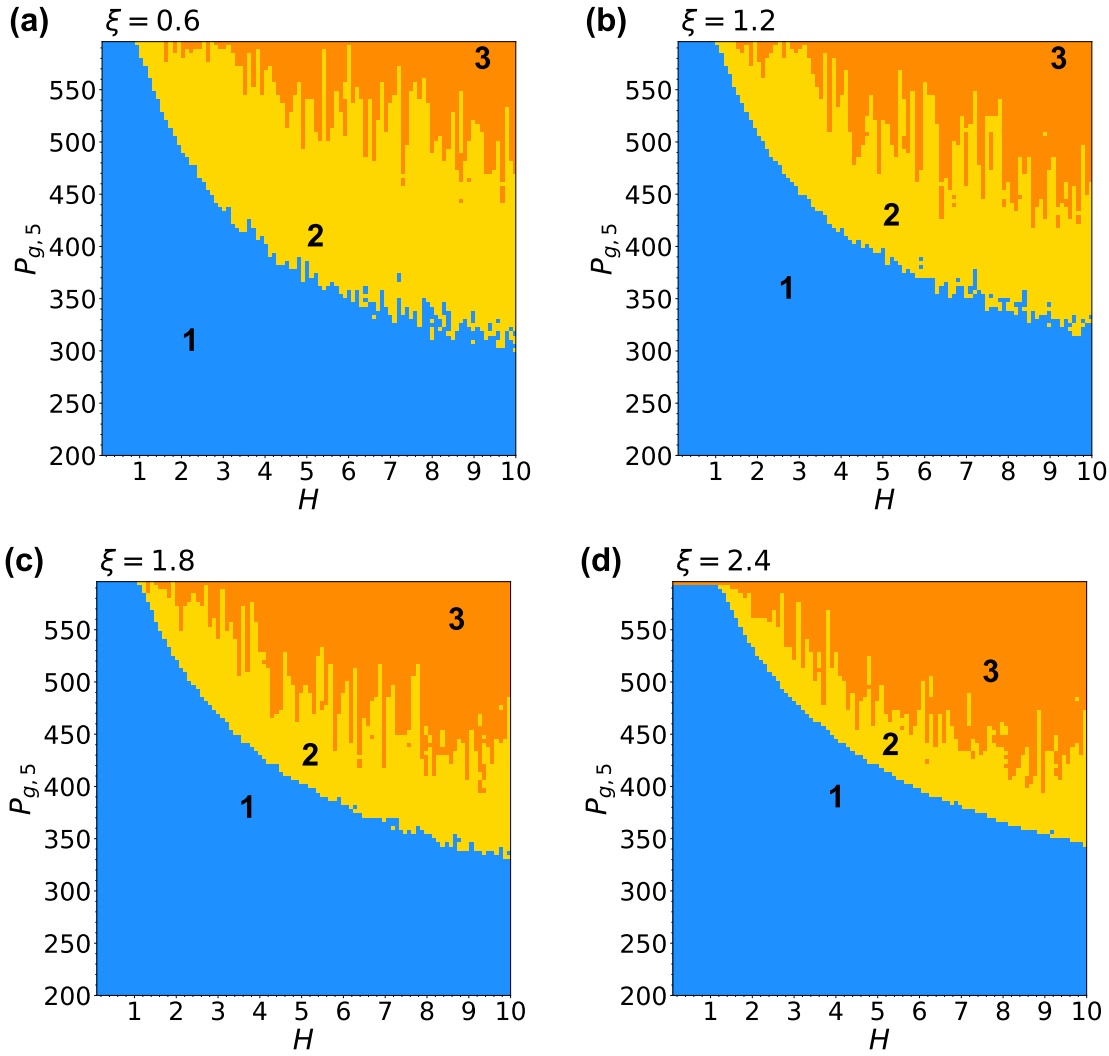

Figure 4.5: Regime maps of the network for the case where we vary the phase-lag of the coupling for the 5th oscillator as shown in Eq. (3). (a) $\xi = 0.6$, (b) $\xi = 1.2$, (c) $\xi = 1.8$, (d) $\xi = 2.4$. The control parameters are the inertia parameter H and the output power of the 5th rotor $P_{g,5}$, with: 1 - area of the synchronous mode (blue); 2 - area of bi-stability (yellow); 3 - area of asynchronous behaviour of one or more oscillators (orange).

Figs 4.5 (a)-(d) show the regions of synchronisation as we increase ξ in Eq. (4.3). Increasing form $\xi = 0.6$ to $\xi = 2.4$, as shown in Figs. 4.5 (a) and (b), expands the region of synchronisation (**1**-blue). However, the expansion of the synchronous region is accompanied by a spreading of asynchronous region (**3**-orange) into the bi-stable region (**2**-yellow). This trend continues as ξ is further increased in Figs. 4.5 (c) and (d) to $\xi = 1.8$ and $\xi = 2.4$, respectively. In Fig. 4.5 (d), the asynchronous region also starts to spread into the (previously) synchronous region, as can be seen at the top left of the control parameter area. This indicates that for high levels of control the network may start to lose synchronicity, even for very low inertia, if the output power of the controlled rotor exceeds $P_{g,5} \gtrapprox 590$. A further increase in $\xi > 2.4$ (not shown) exacerbates this situation, thereby limiting the useful range of the phase-lag control scheme of Eq. (4.3).

4.4 Discussion

Through numerical simulations of various control schemes, applied to an optimised model of power grids [33], we have evaluated their propensity to enhance synchronous behaviour throughout the network.

We first investigated the application of proportional control via the time dependent order parameter, $r(t)$, and Eq. (4.2), through which only the damping coefficient of the excess power rotor (5th rotor) was controlled. In this case we found that the proportional control of the damping of the 5th rotor resulted in a significant improvement in the synchronisation of the entire network. This method was shown to introduce less power dissipation for similar levels of achieved synchronisation and could also be applied to restore synchronisation in a network that has reached a steady state in which one of the rotors rotates faster that the rest.

Building on the idea of nonlinear damping control, as applied to all entities of the network in [33], we found that more effective control could be exerted by applying the same nonlinear damping scheme *only* to the rotor producing the excess power. This, more judicious, application of the nonlinear damping control had the effect of reducing the overall amount of added dissipation needed to establish and maintain synchronicity in the grid. In particular, our comparison of Fig. 4.4 to Fig. 4 of [33] showed that, in order to achieve a similar level of synchronisation in the network, as for the case when the nonlinear damping was applied to *all* the rotors, the 5th rotor could be controlled

with k values that were similar to those used in [33]. We also observed that applying the nonlinear damping to only the 5th rotor, rather than to all the rotors, introduced less dissipation in the network.

We also evaluated the feasibility of applying control via the phase-lags between the 5th oscillator and the rest of the oscillators in the network, according to Eq. (4.3). An increase in the phase-lag gain parameter, up to about $\xi \lessapprox 2.4$, resulted in significantly larger ranges of inertia and output power over which the network would synchronise. Increasing levels of the phase-lag control also expanded the asynchronous region of the control parameters area, and reduced the area of bi-stability. Beyond $\xi = 2.4$ the effectiveness of this type of control is limited, since it starts to introduce asynchronous behaviour at the higher end of the desired control power range, i.e. $P_{g,5} \gtrapprox 590$. It may be possible to extend the phase-lag control to all the interconnected rotors, i.e. in an attempt to further expand the useful operating range of the network. However, to implement such a control scheme, the capacitance of all the transmission lines in the network would have to be varied simultaneously and in real time, according to the order parameter feedback function. While this may be possible in, for example, electronic networks of Josephson junctions [95], it would probably be much more difficult to implement in power grids, due to their much higher power requirements [93].

Chapter 5

Conclusion

As a result of surveying the literature we have discovered that Kuramoto-type models of power grids are much older than was previously thought. Moreover, when Kuramoto presented his (now famous) model in 1975 (Ref. [2]), he was apparently unaware that somewhat more general equations had been used for power grids, much earlier (i.e. the work by Boast and Rector [36].) In the recent literature related to power grids, the model by Boast and Rector has become known as the *Classical Model* [96]. Although a formal link between the Kuramoto model and power grids was made in 2008 by Filaterlla et al. [20], the latter work did not establish the earlier connection that existed. In our present work, we have pointed out, for the first time, the similarities between the Kuramoto-type models and those based on the Classical Model for power grids.

In 2015, Nishikawa and Motter [30] discussed the effects of frustration in power grids. They noted that it is related to the admittance of the transmission lines. However, they described these effects as being negligible, since the admittances of the transmission lines in a real power grid are almost purely inductive. In the Kuromoto-type models of power grids, the purely inductive nature of the admittances means that there should be essentially no phase lags (frustrations) in the sinusoidal coupling terms. For this reason, there are relatively few publications on the effects of frustration on power networks. In our present work, we could identify only four such works: [25, 32–34]. In the work by Arinushkin and Anishchenko [32], the authors studied a Kron reduced model consisting of three oscillators, where every link has a different coupling strength and a significant level of frustration. They tested the tendency for this system to synchronise under various initial conditions, i.e. different initial phases of the oscillators. In order to test our own codes, we started by trying to replicate the results of Ref. [32], and found that

our simulations yielded different results. The results of Ref. [32] were much noisier than our own and indicated that the system would not synchronise in the cases where our simulations showed that it would. This discrepancy was eventually partially resolved, when we discovered, purely by chance, that we could replicate the noise in the results of Ref. [32] by using a too-large fixed time step. Our systematic tests, using different fixed time step sizes, in comparison to an adaptive time step method, confirmed that some of the results presented in Ref. [32] were not clearly properly converged. That being said, although using a larger time step added noise to the plots, we still could not replicate the results found in Ref. [32]. The problem was the large value for the damping parameter that they had used. In order to observe cases where the systems would not synchronise at all, we applied lower damping to the systems. We finally concluded, for the systems discussed in Ref. [32], that there is no oscillatory behaviour, even when a small enough time-step is used to ensure convergence.

In 2023, Botha et al. [25] investigated the propensity of a power grid to synchronise at different levels of frustration and coupling strength. They argued that, despite being typically small in power grids (as noted by Nishikawa and Motter), frustration should not be neglected, since even very small levels of frustration had been shown to affect the behaviour of a network [3, 31]. They found that adding frustration to a network generally impedes synchronisation.

In our follow-up work we investigated how frustration and damping could be used as control methods to induce synchronisation in a power network [26]. Our work was based on the model proposed by Arinushkin and Vadivasova [33], in which nonlinear damping was used as a control method for a network of ten oscillators. In this model, nine of the oscillators had the same natural frequency, and there was one "fast" oscillator, with a higher natural frequency than the others. The nonlinear damping was applied to all ten oscillators, and the level of damping was varied, based on the time dependent order parameter of the system. When the network was completely synchronised (order parameter 1), no additional damping was applied. When the network was completely asynchronous (order parameter close to zero), the maximum amount of damping was applied. In our work, however, we applied the damping only to the "fast" oscillator. We found that when the damping was applied to only the fastest oscillator (rather than to all the oscillators in the network), we could achieve synchronisation using similar damping coefficients. We also tested frustration as a possible control method. We added frustration to the links between the fast oscillator and the rest of the oscillators in the network. We varied the amount of added frustration according to the time-dependent order parameter of the system, as we did with the damping. We found

that adding frustration to the network in this way made the network less sensitive to initial conditions. In other words, the network was less likely to be bi-stable. Rather, it would typically synchronise regardless of the initial conditions, or it would remain asynchronous regardless of initial conditions. Finally, we noted that using damping as a control method involves varying the resistances of the lines in a power network, whereas control via phase-lag (frustration) only involve varying the capacitances of the lines in a network. The latter has the advantage of not introducing additional dissipative effects into the grid.

In 2022, Arinushkin and Vadivasova [34] wrote a third paper on the effects of reactive power on a network. Although we would have liked to reproduce the results of their third paper, it contained insufficient details to allow it to be checked. As in their previous works, the system they considered had been obtained via Kron reduction, and not all the parameters for either the original or the reduced system were published. Thus, we could not perform the Kron reduction ourselves in order to obtain the necessary parameters. Furthermore, our attempts to contact the authors for additional information were unsuccessful – they simply did not respond – which emphasises the need for better data sharing in such publications.

5.1 Future outlook

Recent developments in machine learning have made it possible to make predictions based on large data sets. This technology could potentially be used in power grids. For example, in 2012, Rudin et al. [97] described some machine learning models that can predict the failure ranking and Mean Time Before Failure (MTBF) of distribution feeders and their components in the New York City power grid. One could then apply this knowledge to assist in the prioritisation maintenance and repair work. This allows one to develop proactive maintenance programs using historical data that would have otherwise been underutilised. Another type of machine learning is reservoir computing, which is often trained on time-series data and used to control, for example, chaos in dynamical systems. Recent advances in this field have led to the development of multifunctionality in reservoir computing, i.e. the reservoir can be configured to capture multiple tasks such as when one may have coexisting chaotic attractors [98]. We envisage that a similar approach could be developed to control the synchronicity in power grids. To assess the feasibility of such an approach one could use the same Kuramoto-like models that have been considered in the present work.

One of the challenges encountered in modelling power grids, using Kuramoto-like models, is the difficulty of applying standard numerical continuation methods for their analysis. As we have seen, the models of power grids inherently involve phases, where the phases refer to the actual phases of the voltages and currents of the AC signals in the network. These phases increase with time, and are not in any way bounded. Mathematically, the unbounded phases make it more difficult to apply standard numerical continuation. However, in 2023, Eclerová et al. [99] proposed a solution to this problem by embedding a system of equations governing the behaviour of the phases in a stable generalised system, such that the variables in the generalised system remain bounded. In principle, the same method could be applied to the Kuramoto-like models that we have discussed, provided the systems are not too large. This would allow one to rigorously analyse and detect the bifurcations that occur in these types of power grid models, something which has not yet been done.

Bibliography

[1] Motter, A.E., Myers, S.A., Anghel, M., Nishikawa, T.: Spontaneous synchrony in power-grid networks. Nat. Phys. **9**, 191 (2013). DOI 10.1038/nphys2535. URL http://dx.doi.org/10.1038/nphys2535

[2] Kuramoto, Y.: Self-entrainment of a population of coupled non-linear oscillators. In: H. Araki (ed.) International Symposium on Mathematical Problems in Theoretical Physics, pp. 420–422. Springer Berlin Heidelberg, Berlin, Heidelberg (1975). DOI 10.1007/bfb0013365. URL http://dx.doi.org/10.1007/BFb0013365

[3] Botha, A.E., Ansariara, M., Emadi, S., Kolahchi, M.R.: Chimera patterns of synchrony in a frustrated array of Hebb synapses. Frontiers in Computational Neuroscience **16**, 888019 (2022). DOI 10.3389/fncom.2022.888019. URL https://doi.org/10.3389/fncom.2022.888019

[4] Williams, R.J., Martinez, N.D.: Simple rules yield complex food webs. Nature **404**(6774), 180–183 (2000). DOI 10.1038/35004572. URL http://dx.doi.org/10.1038/35004572

[5] Jeong, H., Tombor, B., Albert, R., Oltvai, Z.N., Barabási, A.L.: The large-scale organization of metabolic networks. Nature **407**(6804), 651–654 (2000). DOI 10.1038/35036627. URL http://dx.doi.org/10.1038/35036627

[6] Strogatz, S.H.: Exploring complex networks. Nature **410**(6825), 268–276 (2001). DOI 10.1038/35065725. URL http://dx.doi.org/10.1038/35065725

[7] Strogatz, S.H.: From Kuramoto to crawford: exploring the onset of synchronization in populations of coupled oscillators. Physica D **143**(1–4), 1–20 (2000). DOI 10.1016/s0167-2789(00)00094-4. URL http://dx.doi.org/10.1016/s0167-2789(00)00094-4

[8] Acebrón, J.A., Bonilla, L.L., Pérez Vicente, C.J., Ritort, F., Spigler, R.: The Kuramoto model: A simple paradigm for synchronization phenomena. Reviews of

Modern Physics **77**(1), 137–185 (2005). DOI 10.1103/revmodphys.77.137. URL http://dx.doi.org/10.1103/revmodphys.77.137

[9] Wiesenfeld, K., Colet, P., Strogatz, S.H.: Synchronization transitions in a disordered Josephson series array. Physical Review Letters **76**(3), 404–407 (1996). DOI 10.1103/physrevlett.76.404. URL http://dx.doi.org/10.1103/physrevlett.76.404

[10] Néda, Z., Ravasz, E., Vicsek, T., Brechet, Y., Barabási, A.L.: Physics of the rhythmic applause. Physical Review E **61**(6), 6987–6992 (2000). DOI 10.1103/physreve.61.6987. URL http://dx.doi.org/10.1103/PhysRevE.61.6987

[11] Vladimirov, A.G., Kozyreff, G., Mandel, P.: Synchronization of weakly stable oscillators and semiconductor laser arrays. Europhysics Letters (EPL) **61**(5), 613–619 (2003). DOI 10.1209/epl/i2003-00115-8. URL http://dx.doi.org/10.1209/epl/i2003-00115-8

[12] Cumin, D., Unsworth, C.: Generalising the kuramoto model for the study of neuronal synchronisation in the brain. Physica D: Nonlinear Phenomena **226**(2), 181–196 (2007). DOI 10.1016/j.physd.2006.12.004. URL http://dx.doi.org/10.1016/j.physd.2006.12.004

[13] Maistrenko, Y.L., Lysyansky, B., Hauptmann, C., Burylko, O., Tass, P.A.: Multistability in the Kuramoto model with synaptic plasticity. Physical Review E **75**(6), 066207 (2007). DOI 10.1103/physreve.75.066207. URL http://dx.doi.org/10.1103/PhysRevE.75.066207

[14] Berner, R., Yanchuk, S., Schöll, E.: What adaptive neuronal networks teach us about power grids. Physical Review E **103**(4), 042315 (2021). DOI 10.1103/physreve.103.042315. URL http://dx.doi.org/10.1103/PhysRevE.103.042315

[15] Grzybowski, J.M.V., Macau, E.E.N., Yoneyama, T.: On synchronization in power-grids modelled as networks of second-order Kuramoto oscillators. Chaos **26**(11), 113113 (2016). DOI 10.1063/1.4967850. URL http://dx.doi.org/10.1063/1.4967850

[16] Sabhahit, N.G., Khurd, A.S., Jalan, S.: Prolonged hysteresis in the Kuramoto model with inertia and higher-order interactions. Physical Review E **109**(2), 024212 (2024). DOI 10.1103/physreve.109.024212. URL http://dx.doi.org/10.1103/PhysRevE.109.024212

[17] Bick, C., Böhle, T., Kuehn, C.: Multi-population phase oscillator networks with higher-order interactions. Nonlinear Differential Equations and Applications NoDEA **29**(6), 64 (2022). DOI 10.1007/s00030-022-00796-x. URL http://dx.doi.org/10.1007/s00030-022-00796-x

[18] Tanaka, H.A., Lichtenberg, A.J., Oishi, S.: First order phase transition resulting from finite inertia in coupled oscillator systems. Phys. Rev. Lett. **78**, 2104–2107 (1997). DOI 10.1103/PhysRevLett.78.2104. URL https://link.aps.org/doi/10.1103/PhysRevLett.78.2104

[19] Tanaka, H.A., Lichtenberg, A.J., Oishi, S.: Self-synchronization of coupled oscillators with hysteretic responses. Physica D: Nonlinear Phenomena **100**, 279-300 (1997). DOI 10.1016/S0167-2789(96)00193-5. URL https://api.semanticscholar.org/CorpusID:55567385

[20] Filatrella, G., Nielsen, A.H., Pedersen, N.F.: Analysis of a power grid using a Kuramoto-like model. The European Physical Journal B **61**(4), 485–491 (2008). DOI 10.1140/epjb/e2008-00098-8. URL http://dx.doi.org/10.1140/epjb/e2008-00098-8

[21] Pikovsky, A., Rosenblum, M., Kurths, J.: Synchronization: A Universal Concept in Nonlinear Sciences. Cambridge University Press (2001). DOI 10.1017/cbo9780511755743. URL http://dx.doi.org/10.1017/CBO9780511755743

[22] Anvari, M., Lohmann, G., Wächter, M., Milan, P., Lorenz, E., Heinemann, D., Tabar, M.R.R., Peinke, J.: Short term fluctuations of wind and solar power systems. New Journal of Physics **18**(6), 063027 (2016). DOI 10.1088/1367-2630/18/6/063027. URL http://dx.doi.org/10.1088/1367-2630/18/6/063027

[23] Rohden, M., Sorge, A., Timme, M., Witthaut, D.: Self-organized synchronization in decentralized power grids. Physical Review Letters **109**(6), 064101 (2012). DOI 10.1103/physrevlett.109.064101. URL http://dx.doi.org/10.1103/physrevlett.109.064101

[24] Rohden, M., Sorge, A., Witthaut, D., Timme, M.: Impact of network topology on synchrony of oscillatory power grids. Chaos **24**(1), 013123 (2014). DOI 10.1063/1.4865895. URL http://dx.doi.org/10.1063/1.4865895

[25] Botha, A., Eclerová, V., Shukrinov, Yu.M., Kolahchi, M.R.: Effects of frustrated interactions on synchronicity in electrical power grids, pp. 53–61. Springer International Publishing (2023). DOI 10.1007/978-3-031-27082-6_5. URL https://doi.org/10.3389/fncom.2022.888019

[26] Olivier, C., Shukrinov, Yu.M., Botha, A.E.: Evaluation of proportional and nonlinear damping control schemes in an optimized power grid. In: 2023 International Conference on Electrical, Computer and Energy Technologies (ICECET), p. 10389565 (2023). DOI 10.1109/ICECET58911.2023.10389565. URL http://dx.doi.org/10.1109/ICECET58911.2023.10389565

[27] Kuramoto, Y.: Chemical Oscillations, Waves, and Turbulence. Springer-Verlag, Berlin (1984). DOI 10.1007/978-3-642-69689-3. URL https://link.springer.com/book/10.1007/978-3-642-69689-3

[28] Sakaguchi, H., Kuramoto, Y.: A soluble active rotator model showing phase transitions via mutual entrainment. Progress of Theoretical Physics **76**(3), 576-581 (1986). DOI 10.1143/PTP.76.576. URL https://doi.org/10.1143/PTP.76.576

[29] Teitel, S., Jayaprakash, C.: Phase transtions in frustrated two-dimensional xy models. Physical Review B **27**(1), 598–601 (1983). DOI 10.1103/physrevb.27.598. URL http://dx.doi.org/10.1103/PhysRevB.27.598

[30] Nishikawa, T., Motter, A.E.: Comparative analysis of existing models for power-grid synchronization. New Journal of Physics **17**(1), 015012 (2015). DOI 10.1088/1367-2630/17/1/015012. URL http://dx.doi.org/10.1088/1367-2630/17/1/015012

[31] Ansariara, M., Emadi, S., Adami, V., Botha, A.E., Kolahchi, M.R.: Signs of memory in a plastic frustrated Kuramoto model of neurons. Nonlinear Dynamics **100**(4), 3685–3694 (2020). DOI 10.1007/s11071-020-05705-4. URL http://dx.doi.org/10.1007/s11071-020-05705-4

[32] Arinushkin, P., Vadivasova: Analysis of synchronous modes of coupled osscilators in power grids. Applied nonlinear dynamics. Izvestiya VUZ **26**(3) (2018). DOI 10.18500/0869-6632-2018-26-3-62-77. URL http://dx.doi.org/10.18500/0869-6632-2018-26-3-62-77

[33] Arinushkin, P., Vadivasova, T.: Nonlinear damping effects in a simplified power grid model based on coupled Kuramoto-like oscillators with inertia. Chaos, Solitons & Fractals **152**, 111343 (2021). DOI 10.1016/j.chaos.2021.111343. URL http://dx.doi.org/10.1016/j.chaos.2021.111343

[34] Arinushkin, P.A., Vadivasova, T.E.: Influence of a reactive power on the dynamics of an ensemble of oscillators simulated by the phase equations with inertia. Radiophysics and Quantum Electronics **65**(1), 59–70 (2022). DOI 10.1007/s11141-022-10193-0. URL http://dx.doi.org/10.1007/s11141-022-10193-0

[35] Tricomi, F.: Integrazione di un'equazione differenziale presentatasi in elettrotecnica. Annali della Scuola Normale Superiore di Pisa, Classe di Scienze 2nd Series, Vol. 2, no 1, pp. 1-20 (1933)

[36] Boast, W.B., Rector, J.D.: An electric analogue method for the direct determination of power system stability swing curves. Transactions of the American Institute of Electrical Engineers **70**(2), 1833–1836 (1951). DOI 10.1109/t-aiee.1951.5060638. URL http://dx.doi.org/10.1109/T-AIEE.1951.5060638

[37] Kimbark, E.W.: Power System Stability, Volume 1, p. 28. John Wiley and Sons (1948). DOI 10.1109/9780470545614.ch2. URL http://dx.doi.org/10.1109/9780470545614.ch2

[38] Fang, X., Misra, S., Xue, G., Yang, D.: Smart grid – the new and improved power grid: A survey. IEEE Communications Surveys & Tutorials **14**(4), 944–980 (2012). DOI 10.1109/surv.2011.101911.00087. URL http://dx.doi.org/10.1109/surv.2011.101911.00087

[39] Morello, R., Mukhopadhyay, S.C., Liu, Z., Slomovitz, D., Samantaray, S.R.: Advances on sensing technologies for smart cities and power grids: A review. IEEE Sensors Journal **17**(23), 7596-7610 (2017). DOI 10.1109/JSEN.2017.2735539. URL http://dx.doi.org/10.1109/JSEN.2017.2735539

[40] Liserre, M., Sauter, T., Hung, J.: Future energy systems: Integrating renewable energy sources into the smart power grid through industrial electronics. IEEE Industrial Electronics Magazine **4**(1), 18–37 (2010). DOI 10.1109/mie.2010.935861. URL http://dx.doi.org/10.1109/mie.2010.935861

[41] Pagani, G.A., Aiello, M.: Power grid complex network evolutions for the smart grid. Physica A: Statistical Mechanics and its Applications **396**, 248–266 (2014). DOI 10.1016/j.physa.2013.11.022. URL http://dx.doi.org/10.1016/j.physa.2013.11.022

[42] Mohsenian-Rad, A.H., Leon-Garcia, A.: Distributed internet-based load altering attacks against smart power grids. IEEE Transactions on Smart Grid **2**(4), 667-674 (2011). DOI 10.1109/TSG.2011.2160297. URL http://dx.doi.org/10.1109/TSG.2011.2160297

[43] Rahman, M.A., Mohsenian-Rad, H.: False data injection attacks with incomplete information against smart power grids. In: 2012 IEEE Global Communications Conference (GLOBECOM), pp.

3153–3158 (2012). DOI 10.1109/GLOCOM.2012.6503599. URL http://dx.doi.org/10.1109/GLOCOM.2012.6503599

[44] Liu, Y., Ning, P., Reiter, M.: False data injection attacks against state estimation in electric power grids. In: Proceedings of the 16th ACM conference on Computer and communications security, vol. 14, pp. 21–32. ACM (2009). DOI 10.1145/1653662.1653666. URL http://dx.doi.org/10.1145/1653662.1653666

[45] Smith, T.B.: Electricity theft: a comparative analysis. Energy Policy **32**(18), 2067–2076 (2004). DOI 10.1016/s0301-4215(03)00182-4. URL http://dx.doi.org/10.1016/S0301-4215(03)00182-4

[46] Li, S., Han, Y., Yao, X., Yingchen, S., Wang, J., Zhao, Q.: Electricity theft detection in power grids with deep learning and random forests. Journal of Electrical and Computer Engineering **2019**, 4136874 (2019). DOI 10.1155/2019/4136874. URL http://dx.doi.org/10.1155/2019/4136874

[47] Chang, L., Wu, Z.: Performance and reliability of electrical power grids under cascading failures. International Journal of Electrical Power & Energy Systems **33**(8), 1410–1419 (2011). DOI 10.1016/j.ijepes.2011.06.021. URL http://dx.doi.org/10.1016/j.ijepes.2011.06.021

[48] Song, J., Cotilla-Sanchez, E., Ghanavati, G., Hines, P.D.H.: Dynamic modeling of cascading failure in power systems. IEEE Transactions on Power Systems **31**(3), 2085–2095 (2016). DOI 10.1109/tpwrs.2015.2439237. URL http://dx.doi.org/10.1109/tpwrs.2015.2439237

[49] Wang, Z., Scaglione, A., Thomas, R.J.: A markov-transition model for cascading failures in power grids. In: 2012 45th Hawaii International Conference on System Sciences, pp. 2115–2124 (2012). DOI 10.1109/HICSS.2012.63. URL http://dx.doi.org/10.1109/HICSS.2012.63

[50] Corso, A., Gambuzza, L.V., Malizia, F., Russo, G., Latora, V., Frasca, M.: Reconstruction of cascading failures in dynamical models of power grids. Journal of Complex Networks **10**(4) (2022). DOI 10.1093/comnet/cnac035. URL http://dx.doi.org/10.1093/comnet/cnac035

[51] Ódor, G., Hartmann, B.: Power-law distributions of dynamic cascade failures in power-grid models. Entropy **22**(6), 666 (2020). DOI 10.3390/e22060666. URL http://dx.doi.org/10.3390/E22060666

[52] Schäfer, B., Yalcin, G.C.: Dynamical modeling of cascading failures in the Turkish power grid. Chaos **29**(9), 093134 (2019). DOI 10.1063/1.5110974. URL http://dx.doi.org/10.1063/1.5110974

[53] Yang, Y., Nishikawa, T., Motter, A.E.: Small vulnerable sets determine large network cascades in power grids. Science **358**(6365), 1524-1542 (2017). DOI 10.1126/science.aan3184. URL http://dx.doi.org/10.1126/science.aan3184

[54] Witthaut, D., Rohden, M., Zhang, X., Hallerberg, S., Timme, M.: Critical links and nonlocal rerouting in complex supply networks. Physical Review Letters **116**(13), 138701 (2016). DOI 10.1103/physrevlett.116.138701. URL http://dx.doi.org/10.1103/physrevlett.116.138701

[55] Braess, D.: Über ein paradoxon aus der verkehrsplanung. Unternehmensforschung Operations Research - Recherche Opérationnelle **12**(1), 258–268 (1968). DOI 10.1007/bf01918335. URL http://dx.doi.org/10.1007/bf01918335

[56] Braess, D., Nagurney, A., Wakolbinger, T.: On a paradox of traffic planning. Transportation Science **39**(4), 446–450 (2005). DOI 10.1287/trsc.1050.0127. URL http://dx.doi.org/10.1287/trsc.1050.0127

[57] Witthaut, D., Timme, M.: Braess's paradox in oscillator networks, desynchronization and power outage. New Journal of Physics **14**(8), 083036 (2012). DOI 10.1088/1367-2630/14/8/083036. URL http://dx.doi.org/10.1088/1367-2630/14/8/083036

[58] Balestra, C., Kaiser, F., Manik, D., Witthaut, D.: Multistability in lossy power grids and oscillator networks. Chaos **29**(12), 123119 (2019). DOI 10.1063/1.5122739. URL http://dx.doi.org/10.1063/1.5122739

[59] Manik, D., Timme, M., Witthaut, D.: Cycle flows and multistability in oscillatory networks. Chaos: An Interdisciplinary Journal of Nonlinear Science **27**(8), 083123 (2017). DOI 10.1063/1.4994177. URL http://dx.doi.org/10.1063/1.4994177

[60] Kuramoto, Y., Davaasambuu, B.: Coexistence of coherence and incoherence in nonlocally coupled phase oscillators. Nonlinear Phenoma in Complex Systems **5**, 380-385 (2002)

[61] Abrams, D.M., Strogatz, S.H.: Chimera states for coupled oscillators. Physical Review Letters **93**(17) (2004). DOI 10.1103/physrevlett.93.174102. URL http://dx.doi.org/10.1103/PhysRevLett.93.174102

[62] Martens, E.A., Thutupalli, S., Fourrière, A., Hallatschek, O.: Chimera states in mechanical oscillator networks. Proceedings of the National Academy of Sciences **110**(26), 10563–10567 (2013). DOI 10.1073/pnas.1302880110. URL http://dx.doi.org/10.1073/pnas.1302880110

[63] Olmi, S., Martens, E.A., Thutupalli, S., Torcini, A.: Intermittent chaotic chimeras for coupled rotators. Physical Review E **92**(3), 030901 (2015). DOI 10.1103/physreve.92.030901. URL http://dx.doi.org/10.1103/physreve.92.030901

[64] Olmi, S.: Chimera states in coupled Kuramoto oscillators with inertia. Chaos **25**(12), 123125 (2015). DOI 10.1063/1.4938734. URL http://dx.doi.org/10.1063/1.4938734

[65] Deng, S., Ódor, G.: Chimera-like states in neural networks and power systems. Chaos: An Interdisciplinary Journal of Nonlinear Science **34**(3) (2024). DOI 10.1063/5.0154581. URL http://dx.doi.org/10.1063/5.0154581

[66] Tumash, L., Olmi, S., Schöll, E.: Effect of disorder and noise in shaping the dynamics of power grids. EPL (Europhysics Letters) **123**(2), 20001 (2018). DOI 10.1209/0295-5075/123/20001. URL http://dx.doi.org/10.1209/0295-5075/123/20001

[67] Schäfer, B., Witthaut, D., Timme, M., Latora, V.: Dynamically induced cascading failures in power grids. Nature Communications **9**(1), 1975 (2018). DOI 10.1038/s41467-018-04287-5. URL http://dx.doi.org/10.1038/s41467-018-04287-5

[68] Haehne, H., Schottler, J., Waechter, M., Peinke, J., Kamps, O.: The footprint of atmospheric turbulence in power grid frequency measurements. EPL (Europhysics Letters) **121**(3), 30001 (2018). DOI 10.1209/0295-5075/121/30001. URL http://dx.doi.org/10.1209/0295-5075/121/30001

[69] Hutcheon, N., Bialek, J.W.: Updated and validated power flow model of the main continental european transmission network. In: 2013 IEEE Grenoble Conference. IEEE (2013). DOI 10.1109/ptc.2013.6652178. URL http://dx.doi.org/10.1109/PTC.2013.6652178

[70] Kumar, A.S., Kouveliotis-Lysikatos, I., Nycander, E., Olauson, J., Marin, M., Amelin, M., Soder, L.: Open nodal power flow model of the nordic power system. In: 2021 IEEE Madrid PowerTech. IEEE (2021). DOI 10.1109/powertech46648.2021.9494886. URL http://dx.doi.org/10.1109/PowerTech46648.2021.9494886

[71] Wang, Z., Elyas, S.H., Thomas, R.J.: Generating synthetic electric power system data with accurate electric topology and parameters. In: 2016 51st International Universities Power Engineering Conference (UPEC), p. 8114145. IEEE (2016). DOI 10.1109/upec.2016.8114145. URL http://dx.doi.org/10.1109/upec.2016.8114145

[72] Elyas, S.H., Wang, Z.: Statistical analysis of transmission line capacities in electric power grids. In: 2016 IEEE Power & Energy Society Innovative Smart Grid Technologies Conference (ISGT), p. 7781263. IEEE Xplore (2016). DOI 10.1109/isgt.2016.7781263. URL http://dx.doi.org/10.1109/isgt.2016.7781263

[73] Plietzsch, A., Kogler, R., Auer, S., Merino, J., Gil-de Muro, A., Liße, J., Vogel, C., Hellmann, F.: Powerdynamics.jl—an experimentally validated open-source package for the dynamical analysis of power grids. SoftwareX **17**, 100861 (2022). DOI 10.1016/j.softx.2021.100861. URL http://dx.doi.org/10.1016/j.softx.2021.100861

[74] Grigg, C., Wong, P., Albrecht, P., Allan, R., Bhavaraju, M., Billinton, R., Chen, Q., Fong, C., Haddad, S., Kuruganty, S., Li, W., Mukerji, R., Patton, D., Rau, N., Reppen, D., Schneider, A., Shahidehpour, M., Singh, C.: The IEEE reliability test system-1996. a report prepared by the reliability test system task force of the application of probability methods subcommittee. IEEE Transactions on Power Systems **14**(3), 1010–1020 (1999). DOI 10.1109/59.780914. URL http://dx.doi.org/10.1109/59.780914

[75] Subcommittee, P.: IEEE reliability test system. IEEE Transactions on Power Apparatus and Systems **PAS-98**(6), 2047–2054 (1979). DOI 10.1109/tpas.1979.319398. URL http://dx.doi.org/10.1109/TPAS.1979.319398

[76] Peyghami, S., Davari, P., Fotuhi-Firuzabad, M., Blaabjerg, F.: Standard test systems for modern power system analysis: An overview. IEEE Industrial Electronics Magazine **13**(4), 86–105 (2019). DOI 10.1109/mie.2019.2942376. URL http://dx.doi.org/10.1109/MIE.2019.2942376

[77] Nakao, H.: Phase reduction approach to synchronisation of nonlinear oscillators. Contemporary Physics **57**(2), 188–214 (2016). DOI 10.1080/00107514.2015.1094987. URL https://doi.org/10.1080/00107514.2015.1094987

[78] Stevenson, W.D.: Elements of power system analysis. McGraw-Hill Companies, MI, Italy (1975)

[79] Kuznetsov, Y.A.: Elements of applied bifurcation theory, 4 edn. Springer International Publishing, Cham, Switzerland (2023). DOI 10.1007/978-3-031-22007-4. URL https://doi.org/10.1007/978-3-031-22007-4

[80] Ren, Q., Zhao, J.: Adaptive coupling and enhanced synchronization in coupled phase oscillators. Physical Review E **76**(1), 016207 (2007). DOI 10.1103/physreve.76.016207. URL http://dx.doi.org/10.1103/PhysRevE.76.016207

[81] Jiang, X., Bai, T., Du, P., Huang, Z.: Nonlinear dynamic behavior and fault diagnosis of rotor-bearing systems subjected to multi-source load unbalance in bulb-type turbine-generator units. Advances in Engineering Software **213**, 104068 (2025). DOI 10.1016/j.advengsoft.2025.104068. URL http://dx.doi.org/10.1016/j.advengsoft.2025.104068

[82] Harris, J.M., Hirst, J.L., Mossinghoff, M.J.: Combinatorics and Graph Theory. Undergraduate Texts in Mathematics. Springer, New York, NY (2010). DOI 10.1007/978-0-387-79711-3. URL https://doi.org/10.1007/978-0-387-79711-3

[83] Watts, D.J., Strogatz, S.H.: Collective dynamics of 'small-world' networks. Nature **393**(6684), 440–442 (1998). DOI 10.1038/30918. URL http://dx.doi.org/10.1038/30918

[84] Zimmerman, R.D., Murillo-Sánchez, C.E., Thomas, R.J.: Matpower: Steady-state operations, planning, and analysis tools for power systems research and education. IEEE Transactions on Power Systems **26**(1), 12-19 (2011). DOI 10.1109/TPWRS.2010.2051168. URL http://dx.doi.org/10.1109/TPWRS.2010.2051168

[85] Clemente-López, D., Munoz-Pacheco, J.M., Rangel-Magdaleno, J.d.J.: Experimental validation of iot image encryption scheme based on a 5-d fractional hyperchaotic system and numba jit compiler. Internet of Things **25**, 101116 (2024). DOI 10.1016/j.iot.2024.101116. URL http://dx.doi.org/10.1016/j.iot.2024.101116

[86] Wolf, A., Swift, J.B., Swinney, H.L., Vastano, J.A.: Determining lyapunov exponents from a time series. Physica D: Nonlinear Phenomena **16**(3), 285-317 (1985). DOI 10.1016/0167-2789(85)90011-9. URL https://www.sciencedirect.com/science/article/pii/0167278985900119

[87] Auer, S., Hellmann, F., Krause, M., Kurths, J.: Stability of synchrony against local intermittent fluctuations in tree-like power grids. Chaos **27**(12), 127003 (2017). DOI 10.1063/1.5001818. URL http://dx.doi.org/10.1063/1.5001818

[88] Coetzee, D., Els, M.: The impact of load shedding on the construction industry in south africa. In: Emerging Trends in Construction Organisational Practices and Project Management Knowledge Areas, p. 268. University of Cape Town, Cape Town (2016)

[89] Das, H., Panda, G.S., Muduli, B., Rath, P.K.: The Complex Network Analysis of Power Grid: A Case Study of the West Bengal Power Network, pp. 17–29. Springer India (2014). DOI 10.1007/978-81-322-1665-0_3. URL https://doi.org/10.1007/978-81-322-1665-0_3

[90] Singh, A.K., Pal, B.C.: Decentralized nonlinear control for power systems using normal forms and detailed models. IEEE Transactions on Power Systems **33**(2), 1160–1172 (2018). DOI 10.1109/tpwrs.2017.2724022. URL https://doi.org/10.1109/tpwrs.2017.2724022

[91] Taher, H., Olmi, S., Schöll, E.: Enhancing power grid synchronization and stability through time-delayed feedback control. Physical Review E **100**(6), 062306 (2019). DOI 10.1103/physreve.100.062306. URL https://doi.org/10.1103/physreve.100.062306

[92] Sieber, J., Omel'chenko, O.E., Wolfrum, M.: Controlling unstable chaos: Stabilizing chimera states by feedback. Physical Review Letters **112**(5), 054102 (2014). DOI 10.1103/physrevlett.112.054102. URL https://doi.org/10.1103/physrevlett.112.054102

[93] Egea-Alvarez, A., Junyent-Ferré, A., Gomis-Bellmunt, O.: Active and Reactive Power Control of Grid Connected Distributed Generation Systems, pp. 47–81. Springer Berlin Heidelberg, Berlin, Heidelberg (2012). DOI 10.1007/978-3-642-22904-6_3. URL http://dx.doi.org/10.1007/978-3-642-22904-6_3

[94] Hairer, E., Nørsett, S.P., Wanner, G.: Solving Ordinary Differential Equations I. Nonstiff Problems, *Springer Series in Computational Mathematics*, vol. 8, 2nd edn. Springer-Verlag, Berlin (1993). DOI 10.1007/978-3-540-78862-1. URL https://doi.org/10.1007/978-3-540-78862-1

[95] Ovchinnikov, Yu.N., Kresin, V.Z.: Networks of Josephson junctions and their synchronization. Phys. Rev. B **88**, 214504 (2013). DOI 10.1103/PhysRevB.88.214504. URL https://doi.org/10.1103/PhysRevB.88.214504

[96] Varaiya, P., Wu, F., Chen, R.L.: Direct methods for transient stability analysis of power systems: Recent results. Proceedings of the IEEE **73**(12), 1703–1715 (1985). DOI 10.1109/proc.1985.13366. URL http://dx.doi.org/10.1109/PROC.1985.13366

[97] Rudin, C., Waltz, D., Anderson, R.N., Boulanger, A., Salleb-Aouissi, A., Chow, M., Dutta, H., Gross, P.N., Huang, B., Ierome, S., Isaac, D.F., Kressner, A., Passonneau, R.J., Radeva, A., Wu, L.: Machine learning for the new york city power grid. IEEE Transactions on Pattern Analysis and Machine Intelligence **34**(2), 328-345 (2012). DOI 10.1109/TPAMI.2011.108. URL https://doi.org/10.1109/TPAMI.2011.108

[98] Du, Y., Luo, H., Guo, J., Xiao, J., Yu, Y., Wang, X.: Multifunctional reservoir computing. Physical Review E **111**(3) (2025). DOI 10.1103/physreve.111.035303. URL http://dx.doi.org/10.1103/PhysRevE.111.035303

[99] Eclerová, V., Přibylová, L., Botha, A.E.: Embedding nonlinear systems with two or more harmonic phase terms near the Hopf-Hopf bifurcation. Nonlinear Dynamics **111**(2), 1537-1551 (2023). DOI 10.1007/s11071-022-07906-5. URL https://doi.org/10.1007/s11071-022-07906-5